



HAL
open science

Cross-linked polymer microparticles with tunable surface properties by the combination of suspension free radical copolymerization and Click chemistry

Yoanh Moratille, Muhammad Arshad, Celine Cohen, Abdelhamid Maali,
Elisabeth Lemaire, Nathalie Sintès-Zydowicz, Eric Drockenmüller

► To cite this version:

Yoanh Moratille, Muhammad Arshad, Celine Cohen, Abdelhamid Maali, Elisabeth Lemaire, et al.. Cross-linked polymer microparticles with tunable surface properties by the combination of suspension free radical copolymerization and Click chemistry. *Journal of Colloid and Interface Science*, In press, 10.1016/j.jcis.2021.09.012 . hal-03353668

HAL Id: hal-03353668

<https://hal.science/hal-03353668>

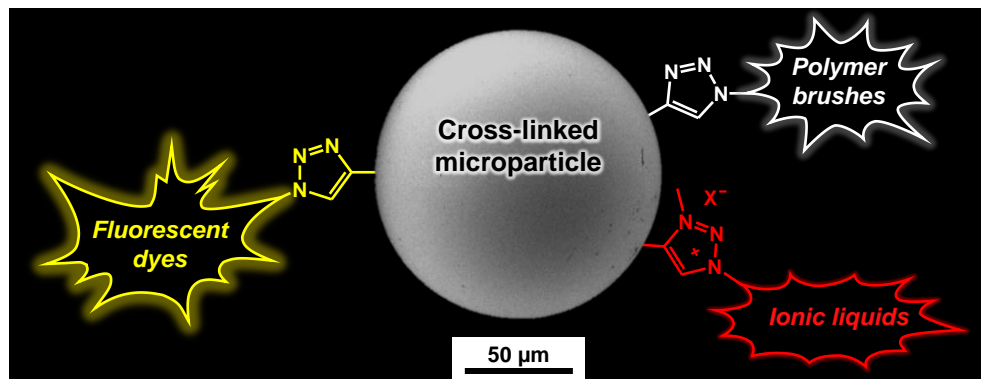
Submitted on 24 Sep 2021

HAL is a multi-disciplinary open access archive for the deposit and dissemination of scientific research documents, whether they are published or not. The documents may come from teaching and research institutions in France or abroad, or from public or private research centers.

L'archive ouverte pluridisciplinaire **HAL**, est destinée au dépôt et à la diffusion de documents scientifiques de niveau recherche, publiés ou non, émanant des établissements d'enseignement et de recherche français ou étrangers, des laboratoires publics ou privés.

[Click here to view linked References](#)

Graphical abstract



Cross-linked polymer microparticles with tunable surface properties by the combination of suspension free radical copolymerization and Click chemistry

Yoanh Moratille ^a, Muhammad Arshad ^c, Celine Cohen ^b, Abdelhamid Maali ^c, Elisabeth Lemaire ^b, Nathalie Sintes-Zydowicz ^{a,*},
Eric Drockenmuller ^{a,*}

^a Univ Lyon, Université Lyon 1, CNRS, Ingénierie des Matériaux Polymères, UMR 5223, F-69003, Lyon, France

^b Université Côte d'Azur, CNRS, InPhyNi-UMR 7010, 06108 Nice Cedex 2, France

^c Univ. Bordeaux, CNRS, LOMA, UMR 5798, F-33405, Talence, France

* Corresponding authors:

Nathalie Sintes-Zydowicz

Université Lyon 1

CNRS

Ingénierie des Matériaux Polymères (UMR 5223)

F-69003 Lyon (France)

Telephone : +33(0)472431002 ; Fax: +33(0)472431249

E-mail: nathalie.sintes@univ-lyon1.fr

Eric Drockenmuller

Université Lyon 1

CNRS

Ingénierie des Matériaux Polymères (UMR 5223)

F-69003 Lyon (France)

Telephone : +33(0)472431983 ; Fax: +33(0)478892583

E-mail: eric.drockenmuller@univ-lyon1.fr

Abstract

We propose a general, versatile and broad in scope two-steps approach for the elaboration of cross-linked polymer microparticles (μ Ps) with tunable surface properties and functionalities. Surface-functionalized cross-linked polymer μ Ps with diameter in the 80 μ m range are prepared by the combination of: 1) suspension free radical copolymerization of styrene, propargyl methacrylate and 1,6-hexanediol dimethacrylate, 2) subsequent covalent tethering of a variety of azide-functionalized moieties by copper(I)-catalyzed azide-alkyne cycloaddition (i.e. rhodamine B fluorescent dye or poly(ethylene glycol) brushes) and, 3) optional *N*-alkylation of the 1,2,3-triazole groups followed by anion exchange reactions to afford covalently-tethered 1,2,3-triazolium ionic liquids with iodide or cresol red as counter-anions. The resulting μ Ps are characterized by laser diffraction, differential scanning calorimetry, as well as by optical, confocal fluorescence, scanning electron and atomic force microscopies. Finally, the rheological properties of concentrated suspensions (volume fractions of 0.40 and 0.44) of the different synthesized μ Ps dispersed in a 1:1 (vol/vol) mixture of polyalkylene glycol and water are studied. The modification of particles surface properties contributes not only to change the stability of the suspensions against flocculation, but also to significantly modify their rheological behavior at high shear stresses. This last result highlights the importance of non-hydrodynamic contact forces in the rheology of non-Brownian suspensions.

Keywords: Functionalized microparticles, suspension copolymerization, Click chemistry, fluorescent microparticles, non-Brownian suspensions, rheology, frictional contacts, adhesion

1. Introduction

Polymer particles are attractive for a wide array of cutting-edge applications such as paints, fillers, cosmetics, coatings, and biomedical devices [1,2]. Polymer microparticles (μ Ps) with diameters above tens of microns are commonly used as model systems for the study of the rheological properties of non-Brownian suspensions (NBSs) [3–7]. Until the 2000s, it was thought that NBSs exhibited universal behavior as long as the particles were spherical and the residual colloidal forces could be neglected when compared to the induced flow forces. Non-Brownian and non-colloidal suspensions were also very often considered to be Newtonian. This claim was supported by the idea that the rheology of suspensions was controlled by hydrodynamic forces which are expected to be proportional to the shear rate. This was tantamount to saying that there was no other characteristic time in the system than the inverse of the shear rate and that therefore the viscosity should not depend on the shear rate (Newtonian behavior). This view was contradicted first by numerous experiments [4,7–9] which clearly showed that non-Brownian suspensions could exhibit shear-thinning behavior and then by the realization of the importance of the role played by direct contact forces between particles in the rheology of NBSs [10–14]. These contacts, which may be frictional, have several important consequences on rheology. First, friction between particles considerably increases the viscosity of suspensions (about 1 order of magnitude for a 50% concentrated suspension) [10,12,14]. Second, recent studies suggest that shear-thinning can be explained by a stress-dependent friction [15–17]. It is therefore of utmost importance to control the surface properties of particles, both for applications involving suspension flows and, from a more fundamental point of view, to be able to conduct quantitative studies on the links between rheology and surface properties. However, most studies on the rheological properties of NBS commonly use rather ill-defined commercial μ Ps which prevent the precise control over their bulk and surface properties. A better understanding of the rheological properties of NBSs and a deepened investigation of the role of involved contact forces requires the access to μ Ps having tailored chemical, physical and structural properties such as: size, size distribution, shape, stiffness, surface roughness and surface chemistry.

Suspension (co)polymerization of functionalized (co)monomers is one of the most suitable and versatile heterogeneous polymerization methods for the elaboration of functional polymer μ Ps in the 10-1000 μ m size range with easily tunable composition as well as dimensional, thermal, mechanical, bulk and surface properties [2,18–25]. However, the scope in terms of chemical functionalities of this fast one-pot approach is limited to functionalities compatible with a radical polymerization process in aqueous dispersed media (i.e. concerns with solubility and tolerance to free radicals). However, a broader range of functional groups can be introduced at the surface of the μ Ps obtained by the suspension copolymerization involving functionalized comonomers (e.g.

alcohol, halide, amine, epoxy, vinyl or alkyne-functionalized comonomers) followed by post-polymerization chemical modification of residual surface functionalities [18,19,25,26]. Robust, efficient and orthogonal ligation reactions, also coined as Click chemistry reactions [27–31], such as the copper(I)-catalyzed azide-alkyne cycloaddition (CuAAC), the ring-opening of epoxide groups (ERO), the hetero Diels–Alder as well as thiol-ene and thiol-yne reactions have been applied to the post-polymerization surface modification of polymer particles with diameters ranging from a few nanometers to 10 μm obtained by dispersion [32], precipitation [33,34], (micro)emulsion [35–37] or seeded [38] polymerization techniques [39]. However, there is a rather limited amount of work related to the chemical modification of the surface of polymer μPs with diameters above tens of microns. Besides the work of Shipp *et al.* who reported cross-linked functional μPs (average size 50 μm) from thiol-ene radical suspension photo-polymerization [40], they mainly consist in the combination microfluidic processes with post-polymerization surface chemical modification using thiol-yne or thiol-ene reactions [41–44]. For instance, Du Prez *et al.* reported the general synthesis of thiol or alkyne-functionalized cross-linked polymer μPs (average size 400 μm) by photopolymerization using a wide range of thiol, alkene and alkyne monomers [41]. The versatility of these μPs was further investigated by thiol-X or CuAAC post-polymerization modification of alkyne or thiol surface functionalities [42]. Du Prez, Ravoo *et al.* introduced bifunctional Janus μPs , particles with different functionalities on opposing poles, in a two-step process consisting of: 1) microfluidic to prepare epoxy, azide or thiol-functionalized polymer μPs (average size 170 μm) and 2) surface modification by “sandwich” microcontact printing employing either ERO, CuAAC or thiol-yne reactions [43,44]. However, to the best of our knowledge surface functionalization of polymer μPs prepared by suspension (co)polymerization using Click chemistry processes has not been reported yet.

Herein, we report free radical suspension copolymerization for preparing alkyne-functionalized cross-linked polymer μPs , with diameter in the 80 μm range, bearing alkyne groups both within and at the surface of the μPs so that they may react with azide-terminated compound through subsequent CuAAC Click reactions. We demonstrate facile, robust and versatile surface modification of these polymer μPs through grafting of azide-terminated polymer brush precursors and azide-functionalized fluorescent dyes. 1,2,3-Triazolium-functionalized μPs were also demonstrated by *N*-alkylation of the 1,2,3-triazole moieties. Finally, the rheological properties of the concentrated NBSs including these surface-functionalized μPs were investigated.

2. Materials and methods

2.1. Materials

Styrene (Merck, 99%), 1,6-hexanediol dimethacrylate (HDDMA, Tokyo Chemical Industry, 98%), propargyl methacrylate (PMA, Alfa Aesar, 98%), lauroyl peroxide (LPO, Fisher Scientific, 95%), poly(vinyl alcohol) (PVA, Acros Organics, $M_w = 88\ 000\ \text{g mol}^{-1}$, degree of hydrolysis = 88%), 4-methoxyphenol (MEHQ, Merck, 98%), sodium hydroxide (NaOH, Carlo Erba, 97%), L-ascorbic acid (Merck, 99%), copper(II) sulfate pentahydrate ($\text{CuSO}_4 \cdot 5\text{H}_2\text{O}$, Merck, 98%), rhodamine B (Merck, 95%), 4-dimethylaminopyridine (DMAP, Merck, 99%), *N,N*-dicyclohexylcarbodiimide (DCC, Merck, 99%), iodomethane (CH_3I , Merck, 99%), cresol red sodium salt (NaCR, Merck, 95%), dichloromethane (DCM, Merck, 99%), *N,N*-dimethylformamide (DMF, Carlo Erba, 99.9%), acetonitrile (CH_3CN , Merck), toluene (Carlo Erba, 99.9%), tetrahydrofuran (THF, Carlo Erba, 99.9%), ethyl acetate (EtOAc, Carlo Erba, 99.8%), methanol (MeOH, Fisher Scientific, 99.8%) and ethanol (EtOH, Carlo Erba, 96%) were used as received. 2-[2-(2-Azidoethoxy)ethoxy]ethanol **1** and α -methoxy- ω -azidoethoxy-poly(ethylene glycol) **3** ($M_w = 37\ 000\ \text{g mol}^{-1}$) were synthesized according to previously published procedures [45].

2.2. Synthesis of alkyne-functionalized cross-linked μPs **MP1**

Spherical cross-linked μPs **MP1** were prepared by suspension free radical copolymerization in a 250 mL jacketed glass reactor equipped with a six-bladed impeller, an argon gas inlet, a condenser and a thermometer. The continuous aqueous phase containing PVA (0.64 g, 0.40 wt%) dissolved in distilled water (160 mL) and the dispersed organic phase containing styrene (28.5 g, 285 mmol), HDDMA (4.26 g, 16.8 mmol), PMA (4.16 g, 33.5 mmol) and LPO (1.35 g, 3.39 mmol) were degassed by argon bubbling during 15 min. The monomer phase was introduced dropwise into the aqueous phase maintained at room temperature (r.t.) while stirring at 820 rpm under argon atmosphere. The stirring was maintained for 30 min at r.t. after which the reactor temperature was raised to 80 °C. Polymerization was allowed to proceed for 3 h before the reaction mixture was cooled down. μPs were isolated by several centrifugation and redispersion cycles using ethanol ($3 \times 100\ \text{mL}$) and deionized water ($5 \times 100\ \text{mL}$) in order to remove residual monomers and adsorbed PVA. Finally, μPs **MP1** were freeze dried to yield a redispersable white powder (25.8 g, 67.6 %).

2.3. Monitoring of monomer conversion during synthesis of μ Ps **MPI** by suspension polymerization

The monomer conversion during the synthesis of μ Ps **MPI** by suspension copolymerization was monitored by gravimetry. The continuous aqueous phase containing PVA (0.64 g, 0.40 wt%) dissolved in distilled water (160 mL) and the dispersed organic phase containing styrene (28.5 g, 285 mmol), HDDMA (4.26 g, 16.8 mmol), PMA (4.16 g, 33.5 mmol) and LPO (1.35 g, 3.39 mmol) were degassed by argon bubbling during 15 min. The monomer phase was introduced dropwise into the aqueous phase maintained at room temperature (r.t.) while stirring at 820 rpm under argon atmosphere. After stirring for 30 min, the emulsion was divided into ca. 6 mL aliquots and filled into glass vials under argon atmosphere. The polymerization was carried out at 80 °C under constant stirring at 820 rpm. At polymerization times ranging from 0 to 3 h, vials were cooled down in an ice bath and quenched by the addition of ca. 6 mL of a 1 wt% solution of MEHQ inhibitor in THF. Each sample was then dried in a vacuum oven at 60 °C until reaching a constant weight. Monomer conversion X was calculated using equation 1:

$$X = \frac{m_p}{m_m} \quad (1)$$

with m_p the mass of dried polymer and m_m the initial mass of comonomers in the aliquot.

2.4. Synthesis of azide-functionalized rhodamine B **2**

A solution of DCC (4.05 g, 19.7 mmol) in CH_2Cl_2 (10 mL) was added dropwise to a solution of 2-[2-(2-azidoethoxy)ethoxy]ethanol **1** (1.38 g, 7.90 mmol), rhodamine B (3.95 g, 8.25 mmol) and DMAP (192 mg, 1.57 mmol) in CH_2Cl_2 (20 mL) maintained at 0 °C. After stirring in the dark at room temperature for 24 h, the crude reaction mixture was purified by column chromatography using a 1:4 mixture of EtOAc and MeOH to yield after evaporation of solvents the rhodamine B azide **2** as a violet solid (2.64 g, 52.5%). ^1H NMR (400 MHz, CDCl_3 , δ): 8.29 (dd, 1H, $J_1 = 1.1$ Hz, $J_2 = 7.9$ Hz, **H_i**), 7.77 (dt, 1H, $J_1 = 1.4$ Hz, $J_2 = 7.5$ Hz, **H_k**), 7.69 (dt, 1H, $J_1 = 1.4$ Hz, $J_2 = 7.7$ Hz, **H_j**), 7.24 (dd, 1H, $J_1 = 1.0$ Hz, $J_2 = 7.5$ Hz, **H_i**), 7.02 (d, 2H, $J = 9.5$ Hz, **H_p**), 6.86 (dd, 2H, $J_1 = 2.5$ Hz, $J_2 = 9.5$ Hz, **H_q**), 6.75 (d, 2H, $J = 2.4$ Hz, **H_s**), 4.13 (m, 2H, **H_f**), 3.56 (m, 16H, **H_b**, **H_c**, **H_d**, **H_e**, **H_u**), 3.31 (m, 2H, **H_a**), 1.28 (t, 12H, $J = 7.1$ Hz, **H_v**). ^{13}C NMR (100 MHz, CHCl_3 , δ): 164.75 (**C_g**), 158.75 (**C_m**), 157.61 (**C_r**), 155.37 (**C_t**), 133.52 (**C_h**), 133.03 (**C_k**), 131.39 (**C_i**), 131.19 (**C_p**), 130.25 (**C_j**), 130.02 (**C_l**), 129.52 (**C_n**), 114.08 (**C_q**), 113.39 (**C_o**), 96.11 (**C_s**), 70.40 (**C_d**), 70.32 (**C_c**), 69.90 (**C_e**), 68.61 (**C_b**), 64.51 (**C_f**), 50.51 (**C_a**), 46.00 (**C_u**), 12.5 (**C_v**). HRMS (ESI) m/z : $[\text{M}]^+$ calcd for $\text{C}_{12}\text{H}_{20}\text{N}_5\text{O}_5$, 600.3179; found, 600.3180.

2.5. *General procedure for the CuAAC functionalization of μ Ps. Preparation of rhodamine-functionalized μ Ps **MP2***

Alkyne-functionalized μ Ps **MP1** (1.0 g, ca. 1.2×10^{-5} mmol of surface alkyne functionalities), rhodamine B azide **2** (1.5 mg, 2.4×10^{-3} mmol), AscNa (200 μ L of a 2.4×10^2 mM aqueous solution, 4.8×10^{-2} mmol) and CuSO₄ (200 μ L of a 12 mM aqueous solution, 2.4×10^{-3} mmol) were added to a 1:1 (vol/vol) mixture of H₂O and EtOH (10 mL) and stirred in the dark for 72 h at 60 °C. The μ Ps were submitted to several centrifugation/dispersion cycles using 1:1 (vol/vol) H₂O/EtOH mixtures (5×50 mL), then H₂O (3×50 mL) and were finally freeze-dried to yield cross-linked μ Ps **MP2** as a pink powder (991 mg, 99.1%).

2.6. *Preparation of poly(ethylene glycol)-grafted μ Ps **MP3***

The general procedure for CuAAC functionalization was applied to μ Ps **MP1** (1.0 g, ca. 1.2×10^{-5} mmol of surface alkyne functionalities), azide **3** (44 mg, 1.2×10^{-3} mmol), AscNa (100 μ L of a 2.4×10^2 mM aqueous solution, 2.4×10^{-2} mmol) and CuSO₄ (100 μ L of a 12 mM aqueous solution, 1.2×10^{-3} mmol) to afford μ Ps **MP3** as a white powder (992 mg, 99.2%).

2.7. *Preparation of tri(ethylene glycol)-grafted μ Ps **MP4***

The general procedure for CuAAC functionalization was applied to μ Ps **MP1** (1.0 g, ca. 1.20×10^{-5} mmol of surface alkyne functionalities) with azide **1** (2.1 mg, 1.2×10^{-2} mmol), AscNa (1.0 mL of a 2.4×10^2 mM aqueous solution, 2.4×10^{-1} mmol) and CuSO₄ (1.0 mL of a 12 mM aqueous solution, 1.2×10^{-2} mmol) to afford μ Ps **MP4** as a white powder (995 mg, 99.5%).

2.8. *Preparation of (1,2,3-triazolium iodide)-functionalized μ Ps **MP5** by N-alkylation*

μ Ps **MP4** (1.0 g, ca. 1.2×10^{-5} mmol 1,2,3-triazole groups), CH₃I (1.5 mL, 2.4×10^{-2} mmol) in CH₃CN (10 mL) was stirred for 72 h at 40 °C. After evaporation of solvent and excess iodomethane under reduced pressure, μ Ps were submitted to several centrifugation/dispersion cycles using CH₃CN (2×50 mL), 1:1 (vol/vol) H₂O/CH₃CN mixtures (2×50 mL), then H₂O (2×50 mL) and were finally freeze-dried to yield cross-linked μ Ps **MP5** as a slightly yellow powder (931 mg, 93.1%).

2.9. Preparation of (1,2,3-triazolium cresol red)-functionalized μ Ps **MP6** by anion exchange

μ Ps **MP5** (500 mg, ca. 6.0×10^{-6} mmol of 1,2,3-triazole groups) and cresol red sodium salt (2.4 mg, 6.02×10^{-3} mmol) in H₂O (10 mL) was heated at 60 °C for 72 h. μ Ps were then submitted to several centrifugation/dispersion cycles using H₂O (5×25 mL) and were finally freeze-dried to yield μ Ps **MP6** as a dark brown powder (989 mg, 98.9%).

2.10. Characterization

Size and size distribution of the μ Ps were measured by laser light diffraction (LD, Mastersizer 2000, Malvern Instruments) in ethanol, as well as dynamic laser light scattering (DLS, Nanosizer ZS, Malvern Instruments). Particle size distribution is defined by the span = $(d_{90}-d_{10})/d_{50}$, where the d_{10} , d_{50} and d_{90} values represent the particle diameter corresponding to the 10%, 50% and 90% cumulative percentage. μ Ps were observed as 0.02 wt% dispersions in water by optical microscopy (OM, BX41, Olympus) with a 10 \times objective, in transmission mode. The morphology of the μ Ps was characterized by scanning electron microscopy (SEM, Merlin Compact, Zeiss) at the Centre Technologique des Microstructures (University of Lyon). The samples were mounted on the sample holder with carbon SEM tape and coated with a thin layer of copper. An accelerating voltage of 1.00 kV was used to be sensitive to the extreme surface morphology. The surface morphology and roughness of the μ Ps were measured using an atomic force microscope (Bioscope AFM equipped with Controller IIIa, Bruker company). A glass slide was cleaned using ultra-pure water and ethanol. It was then coated with a thin layer of epoxy glue (Araldite, Hutsman Advanced Materials). The μ Ps were then manually dispersed on the surface of the epoxy glue. After a few minutes, pressurized nitrogen was thrown onto the surface, so that the non-sticked μ Ps were removed. Several samples were prepared for both μ Ps **MP1** and **MP3**. The AFM was operated in tapping mode using rectangular cantilever (CSG30, NT-MDT Spectrum Instruments) with a tip radius of curvature < 10 nm. After adjusting the laser at the AFM tip, the cantilever was centered on the probed μ P using an optical microscopy setup. The μ Ps were scanned at scan rate of 1 Hz and scan size of 20 \times 20 and 1 \times 1 μ m². The images were processed and analyzed using the “Nanoscope_Analysis” software (Bruker). Confocal fluorescence microscopy was performed at the Centre Technologique des Microstructures (University of Lyon) using a confocal laser scanning microscope (CLSM LSM 800 Zeiss), equipped with 40 \times and 63 \times oil immersion objectives and suitable filter to detect rhodamine B probe (λ_{em} = 565 nm, λ_{ex} = 543 nm). ¹H NMR (400 MHz) and ¹³C NMR (100 MHz) spectra were recorded on a Bruker Avance 400 spectrometer in CDCl₃. Chemical shifts (δ) are given in ppm in reference to the signal of residual CHCl₃ for ¹H NMR (δ = 7.26 ppm) and CDCl₃ for ¹³C NMR (δ = 77.0 ppm). The signals of the different proton and carbon atoms were assigned through additional 1D

and 2D NMR experiments (DEPT, COSY, HSQC, HMBC). Abbreviations for peak multiplicity are s for singlet, d for doublet, t for triplet, dd for doublet of doublet, dt for doublet of triplet and m for multiplet. HRMS experiments were carried out on a MicrOTOF-Q-II spectrometer (Bruker Daltonics, Bremen). Differential Scanning Calorimetry (DSC) was performed using a DSC Q200 (TA Instrument) calibrated with an indium standard. The samples were prepared using sealed pans and the experiments were conducted under a nitrogen purge of 25 mL min⁻¹ on ca. 10 mg. The sample was first heated to 120 °C at a rate of 10 °C min⁻¹. Then, the temperature was decreased to -50 °C at a rate of 10 °C min⁻¹ followed by a second heating to 200 °C at a rate of 10 °C min⁻¹. The glass transition temperature (T_g) was measured at the mid-point of the transition (on the second heating cycle) using the TA Thermal Analysis software. X-ray photoelectron spectroscopy (XPS) experiments were carried out using a K-alpha+ X-ray Photoelectron Spectrometer from Thermo Fisher Scientific equipped with a micro-focused monochromatic Al K α X-ray beam source (1486.6 eV, 400 × 400 μ m² spot size) and a flood gun to compensate for the static charge build-up. The samples were mounted in well generated by metal flat washer glued on the sample holder with tape. All data were acquired at the normal with respect to the plane of the surface. High-resolution core-level spectra of C_{1s}, N_{1s} and I_{3d} were recorded with a 19, 18 and 30 eV pass energy, respectively. The peaks were referenced to C_{1s} at 284.6 eV. The Fityk software was used for data processing. During peak fitting, the N_{1s} curve was split into two groups of three peaks with a ratio of 1:1:1, for the 1,2,3-triazole and 1,2,3-triazolium groups. The shear viscosity of suspensions made either with μ Ps **MP1**, **MP3** or **MP5** was compared at two particle volume fractions: $\phi = 0.40$ and $\phi = 0.44$. The μ Ps were dispersed in a Newtonian fluid made of a 1:1 (vol/vol) mixture of water and polyalkylene glycol (Ucon Lubricant 75-H-90,000, Dow). Polyalkylene glycol is added to water in order to increase the viscosity of the suspending liquid which allows to explore a wide range of shear stress values at low Reynolds numbers. The viscosity of the mixture is 0.96±0.05 Pa.s at 22 °C and the density is the same as that of the μ Ps: 1.045 g cm⁻³. The suspensions were mixed with a spatula until they become homogeneous and then the air bubbles trapped during mixing were removed by placing the suspension containers in an ultrasonic bath for 1 h and then in an oven at 60 °C for 12 h. Viscosity measurements were then carried out in torsional parallel plate geometry, using a controlled-stress rheometer Mars II (Thermo-Scientific). The bottom disk is stationary while a torque (Γ) is applied to the top disk. The suspension was poured on the bottom disc maintained at 22 °C by means of a Peltier element and the gap was set to 1.8 mm. The shear cell was covered with a Plexiglas lid in order to minimize evaporation of the suspending liquid. Parallel-plate geometry has the advantage that shear-induced particle migration is very limited. Indeed, in many cases, shear-induced particle migration gives rise to particle concentration heterogeneities that affect rheometric measurements. This is, for example, the case in a wide-gap cylindrical Couette geometry in

which the particles tend to migrate towards the outer cylinder [46] or in a cone-plane geometry where particles migrate outwards [47]. On the opposite, it has been shown that there was no [47] or very weak [48] migration in a torsional parallel flow so that the apparent viscosity (η_{app}) can be deduced from the ratio of the torque(Γ ,) to the angular velocity of the rotating disc(Ω) using equation 2:

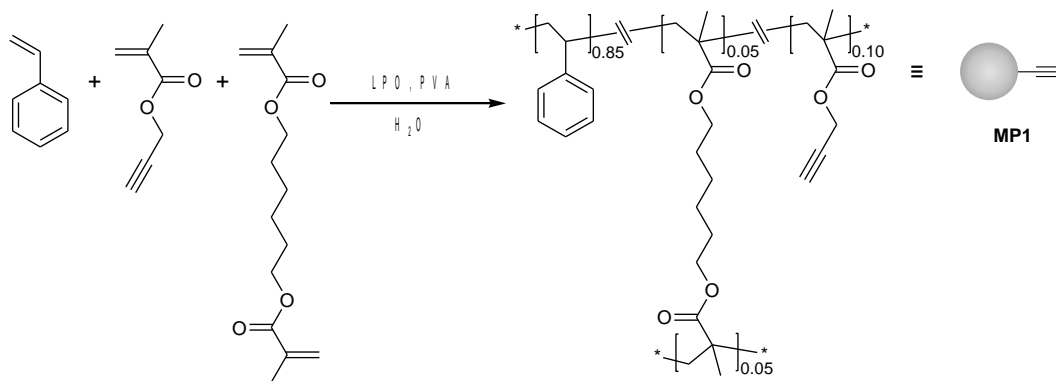
$$\eta_{app} = \frac{2 \times h \times \Gamma}{\pi \times \Omega \times R^4} \quad (2)$$

where $R = 30$ mm is the radius of the rotating disc and $h = 1.8$ mm is the gap between the two discs. The gap has been chosen to be wider than 20 times the particle diameter which is the gap width required for slip and structuring effects to be negligible. This high gap value restricts the range over which shear stress (σ) can be applied. Indeed, it is known that parallel plate flows of suspensions tend to exhibit edge fracture when the magnitude of the second normal stress is larger or of the same order of magnitude as the capillary pressure: $|N_{2c}| \approx 5 \times \gamma / h$ where γ is the surface tension of the suspension [49]. Taking $\gamma \approx 50$ mN m⁻¹, then $|N_{2c}| \approx 100$ Pa. As the magnitude of N_2 is expected to be in the order of a fraction of the shear stress ($N_2 \sim \sigma/2$), the upper limit of the shear stress range is of the order of a few hundred Pa.

The second difficulty of using a rotating parallel plate geometry is that the shear rate is not constant but increases from zero at the center to $\dot{\gamma}_R = \Omega \times R / h$ at the rim which can be problematic for a fluid whose viscosity varies with shear rate, as is the case for concentrated non-Brownian suspensions. However, this problem can be overcome by introducing a Rabinovitch correction [50]:

$$\eta = \eta_{app} \left(1 + \frac{1}{4} \frac{d \ln \eta_{app}}{d \ln \dot{\gamma}_R} \right) \quad (3)$$

Finally, it must be checked that the measurements are carried out when the viscosity has reached its steady value. The viscosity of a suspension is closely related to its microstructure and the microstructure only reaches its steady state when the deformation to which the suspension has been subjected has exceeded a few units [51]. Therefore, to meet this requirement, shear stress steps were applied rather than a continuously growing shear stress and to verify that, for each value of the stress, the suspension was sheared over a strain of several units.



Scheme 1. Synthesis of alkyne-functionalized cross-linked μ Ps **MP1**.

3. Results and discussion

3.1. Synthesis of alkyne-functionalized cross-linked μ Ps

Cross-linked alkyne-functionalized μ Ps **MP1** (Scheme 1) were obtained by suspension free radical copolymerization of styrene (85 mol%), PMA (10 mol%) and HDDMA cross-linker (5 mol%) using PVA as stabilizer (0.4 wt% with respect to the water continuous phase) and LPO as initiator (1 mol% with respect to comonomers). The monomers/ H_2O volume ratio was fixed at 1:4 and the polymerization was carried out at 80 °C for 3 h. Gravimetric monitoring as a function of polymerization time has shown that after a ca. 5 min inhibition period an almost complete conversion of the monomers was reached after 3 h of reaction at 80 °C (Fig. 1). After elimination of the surfactant and monomer residuals by centrifugation/dispersion cycles using ethanol and deionized water followed by freeze-drying, alkyne-functionalized cross-linked μ Ps **MP1** were obtained in 68% yield as a white powder that could be readily redispersed in water, EtOH, and CH_3CN . As shown by DSC analysis of μ Ps **MP1** (Fig. S2 in the Supporting Information) no exotherm was found, indicating the absence of residual monomers. Besides, a T_g value of 94 °C was afforded thus confirming a glassy state at room temperature. It is worth mentioning that the obtained T_g value is in good agreement with the value calculated from the Fox's law ($T_g = 92$ °C) using the molar ratios of each comonomers in the feed and the T_g values previously reported for the corresponding homopolymers ($T_g = 100$, 55 and 28 °C for homopolymers of styrene, PMA and HDDMA) [52–54].

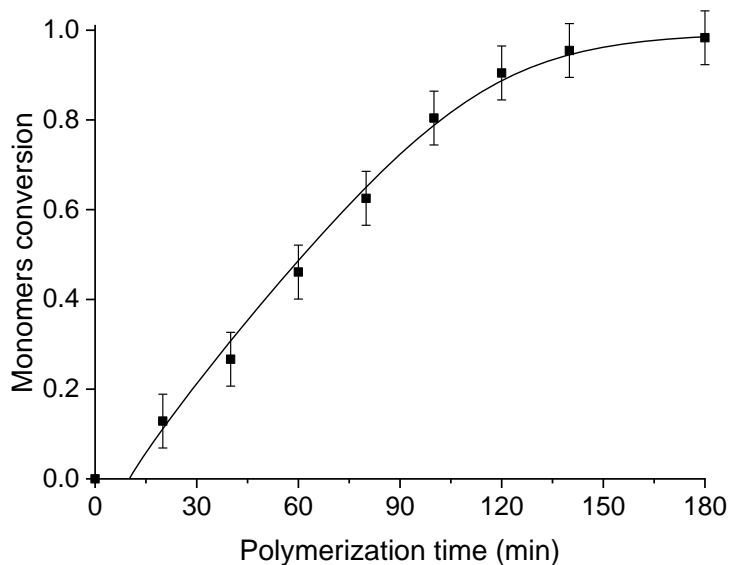


Fig. 1. Monomers conversion as a function of polymerization time at 80 °C during the synthesis of μ Ps **MP1** by suspension polymerization (The solid line is intended only as a guide to the eye).

Optical microscopy confirmed the spherical shape of μ Ps **MP1** with diameters ranging from ca. 20 to 160 μ m (Fig. 2a-c). This was corroborated by LD (Fig. 2d) as μ Ps **MP1** exhibit d_{50} of 80 μ m with a span of 0.74. Replicas of the synthesis of μ Ps **MP1** showed almost identical size and size distribution (Fig. 2d), attesting for the robust and highly reproducible particle formation process. The spherical shape and low surface roughness of μ Ps **MP1** was also confirmed by SEM (Fig. 3a-b). However, at higher magnification a low amount of adhered nanoparticles (nPs) with ca. 20-200 nm diameter could be observed at the surface of μ Ps **MP1** (Fig. 3c). Such nPs, also coined as “emulsion particles”, result from the decomposition of initiator in the aqueous phase into free radicals, reacting with comonomers dissolved in the aqueous phase [55]. The formation of these emulsion particles is heavily dependent on the partial water solubility of comonomers and initiator, as well as the concentration of surfactant [56,57]. Here, methacrylate-based and styrene monomers as well as initiator with very low water solubility limit excessive formation of such secondary particles (Table S1). After polymerization, DLS of the unwashed water phase showed emulsion particles of ca. 60-500 nm diameter (Fig S3). Most emulsion particles were discarded by repeated washings and centrifugations cycles in EtOH and deionized water, however some remained permanently attached to the surface of μ Ps due to the difunctional nature of the HDDMA cross-linker (Fig 3c). Also, PVA has long been identified as a cause of interparticle bridging and can occur by adsorption between the hydrophobic acetate blocks and the surface of hydrophobic polymer particles [58,59] or covalent bonds, in the presence of free radical, reactive sites may form on PVA leading to subsequent grafting to the particles [60]. The surface morphology of the different μ Ps by AFM is further discussed into more details in section 3.2.

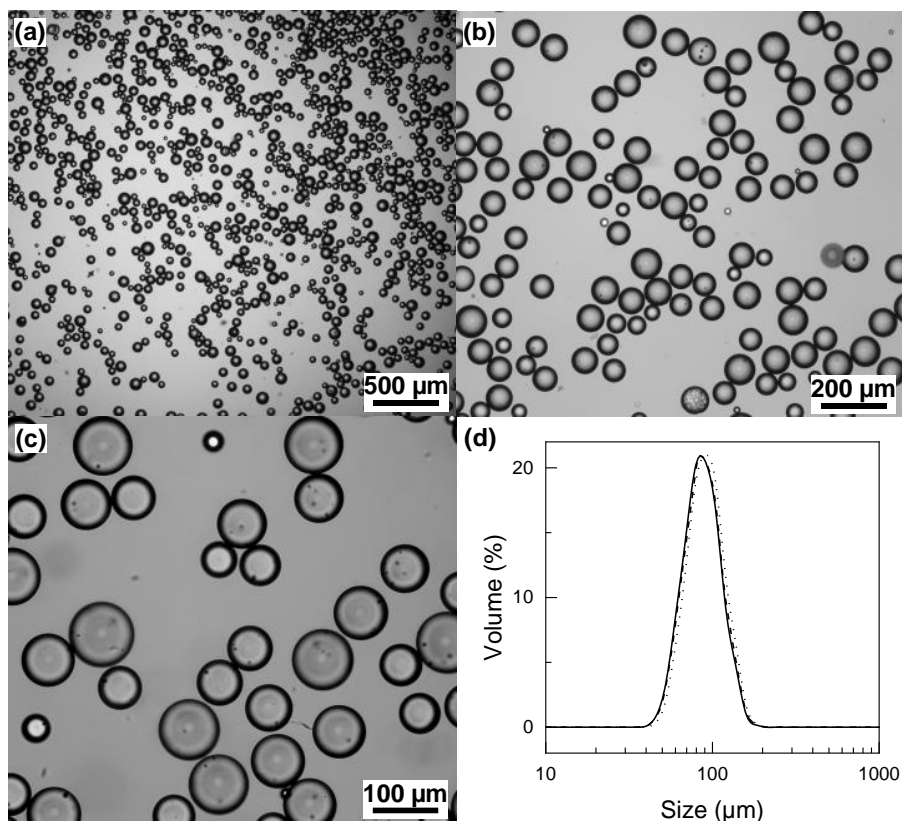


Fig. 2. (a-c) Optical microscopy images of alkyne-functionalized μ Ps **MP1**. (d) LD size distribution of μ Ps **MP1** (solid line) as well as μ Ps **MP1** replica (dotted line) and poly(ethylene glycol)-grafted μ Ps **MP3** (dashed line).

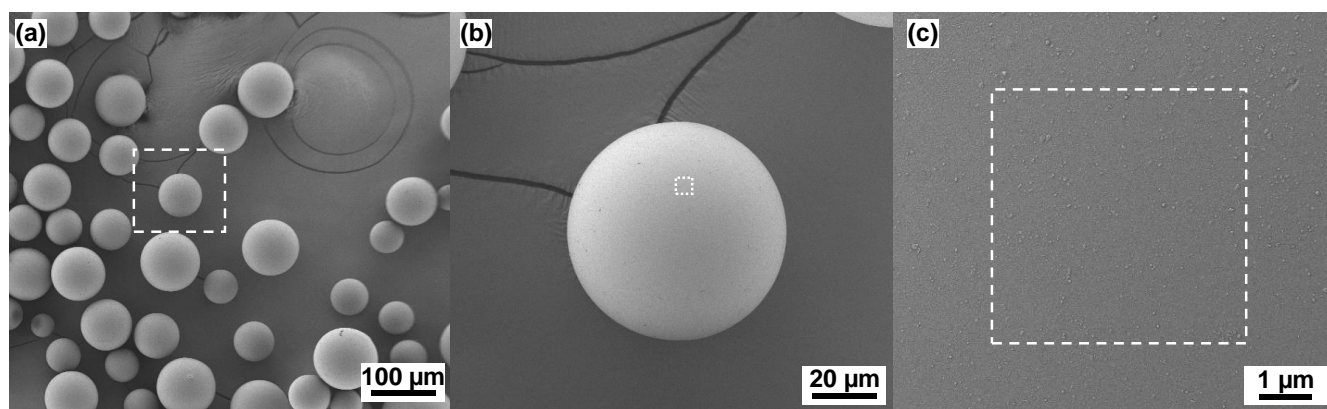
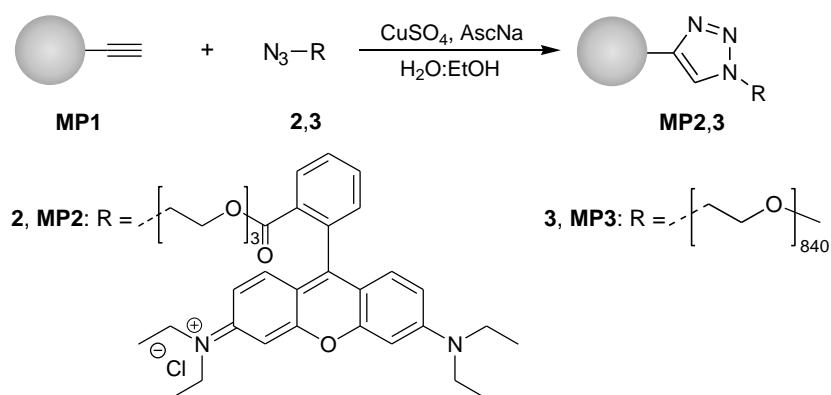


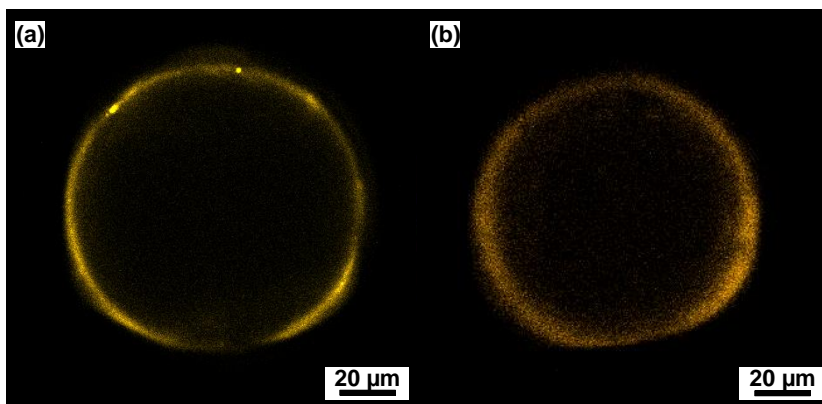
Fig. 3. (a-c) SEM images of alkyne-functionalized μ Ps **MP1** at different magnifications.

μ Ps **MP1** appeared redispersible and insoluble in water, EtOH, CH₃CN and DCM at room temperature, attesting for the efficient cross-linking of the polymer. The cross-linking degree, and so the swelling, of the μ Ps is critical as it dictates the accessibility of bulk and surface alkyne groups during subsequent chemical modifications. The swelling of μ Ps **MP1** ($S = V_S/V_W$) was thus calculated by comparing the volume of the μ Ps measured by LD after 72 h of soaking in water (V_W) and in different solvents (V_S). For poor solvents, the swelling was moderate ($S = 112$ and 116% for EtOH and CH₃CN, respectively) while for DCM, a good solvent for PS, the more significant swelling ($S = 239\%$) without any dissolution of the μ Ps attested the high cross-linking density of the μ Ps **MP1** (Fig. S4).



Scheme 2. Synthesis of rhodamine-functionalized μ Ps **MP2** and poly(ethylene glycol)-grafted μ Ps **MP3** by CuAAC post-polymerization chemical modification of alkyne-functionalized μ Ps **MP1**.

3.2. Surface modification of alkyne-functionalized μ Ps



4.

Fig. 4. Confocal fluorescence microscopy of equatorial cross-sections (5 μ m thick) of (a) rhodamine-functionalized μ Ps **MP2** and (b) cresol red-functionalized μ Ps **MP6**.

The alkyne-functionalized μ Ps **MP1** were used as clickable scaffolds for their surface chemical modification by CuAAC using rhodamine B azide **2** and α -methoxy- ω -azidoethoxy-poly(ethylene glycol) **3** (Scheme 2). Since 1) alkyne groups are distributed at both the core and the surface of the μ Ps, 2) azides **2** and **3** are hydrosoluble, and 3) μ Ps **MP1** do not swell in water and in EtOH, the CuAAC surface modifications were carried out under hydro-alcoholic conditions using CuSO₄/sodium ascorbate as catalytic system and a 1:1 (vol/vol) H₂O/EtOH as dispersing medium. These conditions ensured that the chemical modification almost exclusively occurred at the μ Ps surface [61]. Azides **2** and **3** were introduced in large excess (100 equiv.) with respect to the estimated amount of surface alkyne groups in μ Ps **MP1** estimated using Eq. S3 and S5.

A first proof of the CuAAC chemical modification of the surface of μ Ps **MP1** was provided by confocal fluorescence microscopy of μ Ps **MP2** after tethering fluorescent azide-functionalized rhodamine B **2**. Azide-functionalized fluorescent dye **2** was synthesized through DCC-mediated esterification of rhodamine B and 2-[2-(2-azidoethoxy)ethoxy]ethanol **1** (Scheme S1). The structure and purity of **2** was assessed by NMR spectroscopy (Fig. S5 and Fig. S6) and by electrospray ionization high-resolution mass spectrometry. The absorption and emission spectra of **2** ($\lambda_{\text{abs}} = 560$ nm, $\lambda_{\text{em}} = 586$ nm in water) was obtained by UV-vis spectroscopy (Fig. S7). Azide-functionalized fluorescent dye **2** was tethered at the surface of μ Ps **MP1** by CuAAC to afford μ Ps **MP2** (Scheme 2). After thorough removal of non-reacted azide **2**, analysis of equatorial cross-section of μ Ps **MP2** by confocal fluorescence microscopy showed the presence of a yellow fluorescent ring, demonstrating an effective surface anchoring of azide **2** (Fig. 4a). Due to the low swelling of the μ Ps in the EtOH and water, the width of the fluorescent ring (*ca.* 3 μ m) is most probably due to a “fluorescence glare” stemming from structures above and below the focal plane rather than to the actual depth of the grafting reaction. The Z-stacks obtained by confocal fluorescence microscopy were used for the reconstruction and segmentation of μ Ps **MP2** (Video S1).

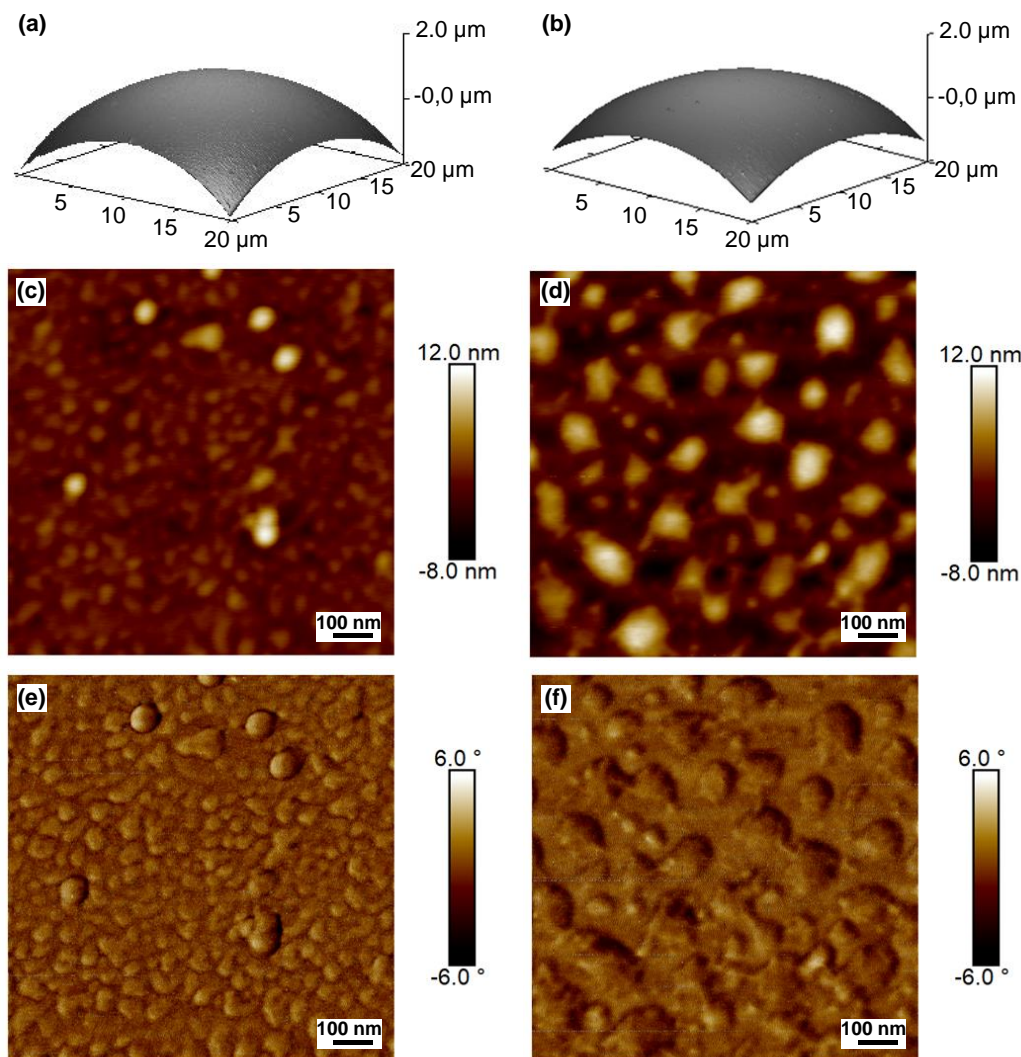
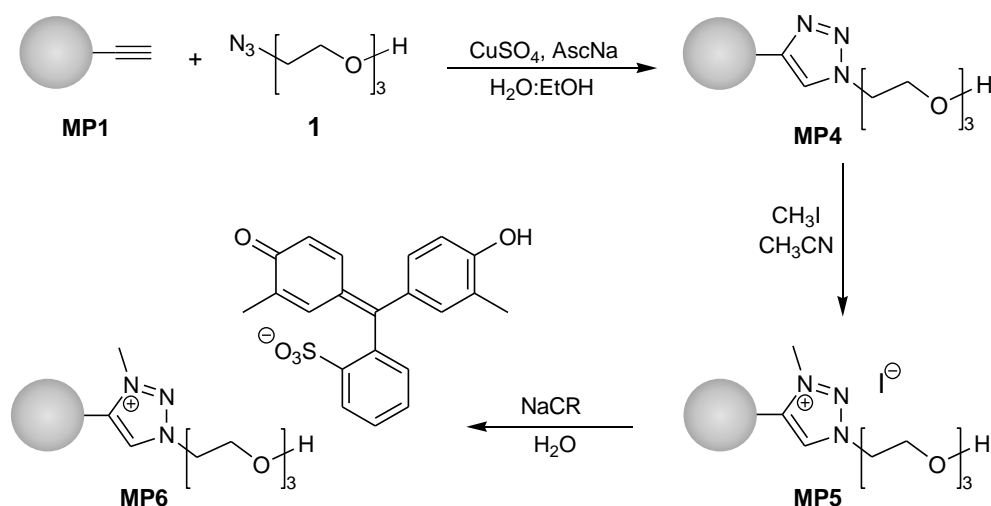


Fig. 5. AFM (a-b) ($20 \times 20 \mu\text{m}^2$) 3D surface reconstruction, (c-d) ($1 \times 1 \mu\text{m}^2$) height and (e-f) ($1 \times 1 \mu\text{m}^2$) phase images of (a,c,e) alkyne-functionalized μPs **MP1** and (b,d,f) poly(ethylene glycol)-grafted μPs **MP3**.

Poly(ethylene glycol)-grafted μPs **MP3** were also obtained by the CuAAC tethering of α -methoxy- ω -azidoethoxy-poly(ethylene glycol) **3** ($M_n = 37 \text{ kg mol}^{-1}$) at the surface of μPs **MP1** (Scheme 2). Both LD (Fig. 2d) and SEM (Fig. S8a-b) analyses of μPs **MP3** confirmed that size, size distribution and surface morphology were comparable to those of alkyne-functionalized μPs **MP1**.

The surface morphology of μ Ps **MP1** and **MP3** was investigated in more details by AFM (Fig. 5). Besides the presence of previously mentioned emulsion particles of ca. 30 nm in diameter, μ Ps **MP1** presented low surface roughness with a root mean square (RMS) roughness of 2.2 nm (Fig. 5c), consistent with previous SEM observations (Fig. 3c). However, phase images of **MP1** showed a surface with distinct domains, suggesting areas with different concentration of PS, PPMA and PHDDMA (Fig. 5e). Conversely, the surface of μ Ps **MP3** showed an increased RMS roughness of 3.6 nm and the apparition of small, globular domains of ca. 20-150 nm in diameter (Fig. 5d). The low phase contrast between the globular-like morphologies and the background suggests that the entire surface is homogeneously covered by PEG brushes (Fig. 5f). These features have been frequently observed in the literature concerning PEG brushes “grafted-to” planar silicon substrates [62].



Scheme 3. Synthesis of 1,2,3-triazolium-functionalized μ Ps **MP5** and **MP6** by *N*-alkylation and ion exchange reaction.

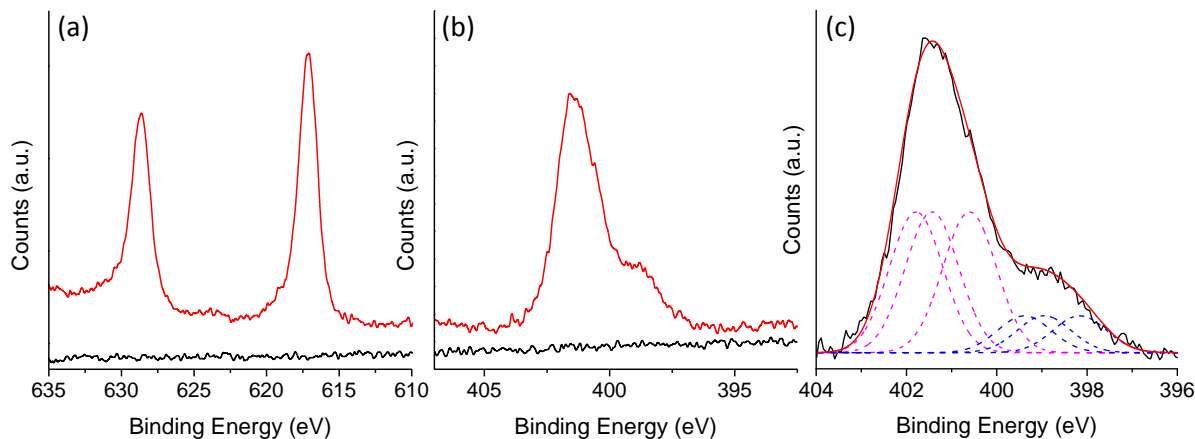


Fig. 6. High resolution (a) I_{3d} and (b) N_{1s} of spectra of alkyne-functionalized μ Ps **MP1** (black line) and (1,2,3-triazolium)-grafted μ Ps **MP5** (red line). (c) Peak fitted high resolution of N_{1s} spectrum of μ Ps **MP5**. The N_{1s} curve (black line) was split into 3 signals with 1:1:1 area ratio for the 1,2,3-triazole groups (blue dashed lines) and 3 signals with 1:1:1 area ratio for the 1,2,3-triazolium groups (pink dashed lines). The red line corresponds to the sum of the different contributions.

A last sequence of surface chemical modifications was applied to alkyne-functionalized μ Ps **MP1** in order to afford cross-linked polystyrene μ Ps having surface tethered 1,2,3-triazolium-based ionic liquids (Scheme 3). Initially, CuAAC reaction between 2-[2-(2-azidoethoxy)ethoxy]ethanol **1** and alkyne functionalities from the surface of μ Ps **MP1** afforded 1,2,3-triazole-functionalized μ Ps **MP4**. Subsequent *N*-alkylation of 1,2,3-triazole groups in acetonitrile for 72 hours at 40 °C using a large excess of methyl iodide (i.e. 2000 equiv. according to initial surface alkyne groups) yielded (1,2,3-triazolium iodide)-functionalized μ Ps **MP5**. SEM of **MP4** and **MP5** (Fig. S8c-f) showed that the surface morphology remained unchanged after the sequential chemical modifications. The occurrence of this surface chemical modification sequence was demonstrated by XPS analysis of (1,2,3-triazolium iodide)-functionalized μ Ps **MP5**. First, high-resolution I_{3d} spectra of μ Ps **MP1** and **MP5** provided a clear evidence of the formation of surface tethered 1,2,3-triazolium iodides through the appearance of $I_{3d5/2}$ and $I_{3d3/2}$ peaks (at 618.1 and 629.4 eV, respectively) characteristic of iodine anions (Fig. 6a). This was corroborated by the high-resolution N_{1s} spectra with the appearance of a main peak at 401.4 eV and a shoulder peak at 398.8 eV typical of 1,2,3-triazolium and 1,2,3-triazole groups, respectively (Fig. 6b) [63]. Decomposition of the averaged high resolution N_{1s} spectrum into three peaks with 1:1:1 ratio for 1,2,3-triazole and 1,2,3-triazolium groups allowed to quantify the presence of ca. 20 mol% of 1,2,3-triazole groups remaining after the *N*-alkylation step (Fig. 6c). This appeared rather surprising according to the large excess of methyl iodide and the

long reaction time. This could not be explained by higher swelling of the μ Ps during the CuAAC step (in hydroalcoholic medium) than the *N*-alkylation step (in acetonitrile) (Fig. S4). A more likely explanation is the de-*N*-alkylation reaction of the 1,2,3-triazolium groups and the reactivity of iodide groups during XPS analysis which has been previously reported [64]. Finally, anion exchange reaction between the surface 1,2,3-triazolium iodide groups of μ Ps **MP5** and cresol red sodium salt fluorescent dye afforded fluorescently labeled μ Ps **MP6**. The presence of cresol red fluorescent counter-anion was again confirmed by confocal fluorescence microscopy and appeared as a wide yellow fluorescent ring of ca. 10 μ m surrounding μ Ps **MP6** (Fig. 4b). The apparent surface localization of fluorescence suggests that the anion exchanged occurred and attests for the efficiency of the *N*-alkylation step. A possible reason for the additional width may arise from the size difference of the selected particles, smaller local radius of curvature of the particle leads to a wider fluorescence glare intensity.

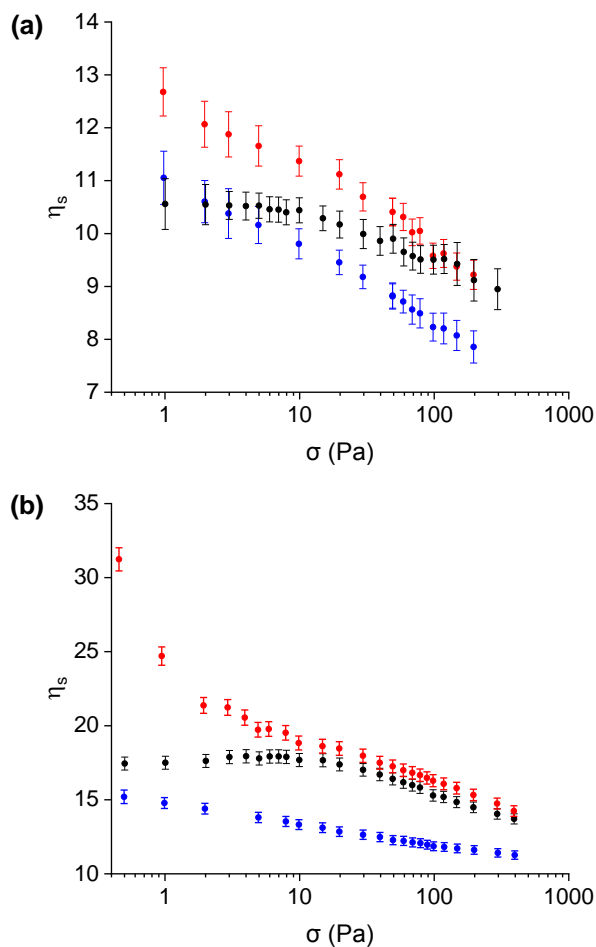


Fig. 7. Shear viscosity vs shear stress for suspensions composed of alkyne-functionalized μ Ps **MP1** (red dots), poly(ethylene glycol)-grafted μ Ps **MP3** (blue dots) and (1,2,3-triazolium iodide)-functionalized μ Ps **MP5** (black dots) for particle volume fractions of (a) 0.40 and (b) 0.44. The viscosity of the suspending liquid is 0.96 Pa.s.

4.1. Influence of surface functionalization on the rheological properties of NBSs of μ Ps **MP1**, **MP3** and **MP5**

In this section, the effect of μ Ps surface properties on the rheology of NBS was investigated. Numerical simulations carried out over the last decade have shown the crucial role played by direct particle contact forces in the rheology of NBS [12,65,66]. All the results of numerical simulations show that the viscosity of concentrated NBSs increases significantly when the coefficient of interparticle friction increases in the range [0-1]. On the contrary, these simulations show a very small impact of particle roughness on the viscosity of the suspensions. This result is in apparent contradiction with the experimental results of Tanner & Dai [67–69] who studied the viscosity of suspensions of rough PS, PMMA or glass μ Ps. These results have shown a significant increase in

viscosity with the increase of the particles surface roughness. These contradictory results may stem from the fact that it is quite experimentally challenging to vary independently the friction coefficient and roughness. To decouple the influence of these two parameters, we have chosen here to compare the behavior of NBSs with μ Ps having equivalent size, size distribution and roughness but strikingly different surface functionalities.

Fig. 7 shows the variation of the shear viscosity with shear stress for suspensions composed of either μ Ps **MP1**, **MP3** or **MP5** for two particle volume fractions: $\phi = 0.40$ and 0.44 . The influence of surface chemistry on suspension viscosity is clearly visible, especially for the most concentrated suspensions ($\phi = 0.44$, Fig. 7b). Recent studies have shown that shear-thinning observed in concentrated NBSs was due either to the presence of adhesion forces between particles [70] or to the decrease in the interparticle friction coefficient when the shear stress increases [15,17] or both [71]. These two effects lead to variations in viscosity with shear stress that have very different patterns. In particular, in the case of shear-thinning induced by the presence of adhesive forces between particles, the viscosity decrease is expected to be all the more marked the smaller the stress. Inspection of Fig. 7b shows the presence of two distinct shear-thinning regimes for the **MP1**-based suspension: one at low shear stress (typically observed for $\sigma < 5$ Pa) and another regime where the viscosity decreases less rapidly for $\sigma > 10$ Pa. By comparing this curve with that obtained for the **MP5**-based suspension, it is clear that the addition of a surface charge leads to the suppression of the first shear-thinning regime (at low stress values). The electrical charge carried by the particles results in an electrostatic force barrier which prevents particles from coming into contact due to van der Waals forces. The weak shear-thickening that is observed at low stress values ($\sigma \lesssim 3$ Pa) can probably be explained by the promotion of interparticle contacts as the shear stress is ramped up from zero. This scenario has been proposed to explain discontinuous shear-thickening (DST) in stabilized suspensions [72]. In DST, the viscosity jumps across non-shear-thickened to shear-thickened regime can be of several orders of magnitude. The shear-thickening here observed is much less spectacular, but one has to keep in mind that DST is only observed for very concentrated suspensions ($\phi \gtrsim 0.54$). For lower particle volume fractions, DST turns out to CST with a continuous -and rather limited- increase of viscosity with stress [73,74]. So the shear-thickening here observed can be interpreted in terms of the competition between the flow-induced forces which push the particles against each other and the repulsive forces (here of electrostatic nature) which tend to prevent contacts and is then the evidence that the (1,2,3-triazolium iodide)-functionalization of the μ Ps enabled to stabilize the suspension.

Beyond a typical stress of about 10 Pa, the rheograms obtained either with **MP1** or **MP5**-based suspensions converge and show a similar shear-thinning trend that is controlled by interparticle frictional forces.

The **MP3**-based suspension behaves in a different way with a continuous regular shear-thinning over more than three stress decades. Moreover, the viscosity is significantly lower than that of the other two suspensions. This result was anticipated since brush-modified surfaces are known to exhibit a much lower friction coefficients than bare surfaces (see [75] for a review). The typical values of friction coefficient for PEG-grafted surfaces are in the range [0.01-0.1] while the friction coefficient of bare polystyrene is of the order of [0.3-0.5]. Thus, grafting polymer brushes on particle surface is an efficient way to decrease NBS viscosity. Therefore, rheometric measurements have shown significant impact of surface properties of particles on rheology even though, given the particle size (80 μm), the studied suspensions are deemed “non-colloidal”. These observations support the idea that a fine characterization of particle properties is necessary to both predict and understand the rheological behavior of NBS. From a practical point of view, the sensitivity of NBS rheology to particle surface properties opens perspectives in application fields where it is necessary to optimize the rheological properties.

5. Conclusions

This study demonstrates the successful synthesis of large alkyne-functionalized cross-linked μPs via suspension copolymerization and their subsequent surface modification by Click chemistry. Using this general surface grafting strategy poly(ethylene glycol)-grafted μPs were first fabricated. The visualization of the μPs carried out with SEM showed spherical shape and smooth surface. Well-defined and homogeneous surface-tethered PEG brushes observed by AFM and changes to the rheological properties of the resulting dense suspensions demonstrated successful surface modification. In an additional approach, cross-linked μPs with surface-tethered 1,2,3-triazolium ionic liquids were obtained by CuAAC of azide-functionalized tri(ethylene glycol) and subsequent *N*-alkylation of the 1,2,3-triazole groups. Their surfaces were characterized by XPS, confocal fluorescence microscopy and rheological measurement of surface-modified μPs . This represents a general, straightforward and effective method to afford cross-linked polymer μPs with a broad range of surface properties. We have shown that the grafting of hydrophilic polymers or ionic liquid to initially hydrophobic cross-linked polymer μPs is a facile approach to provide the tuning of the rheological properties of the resulting Non-Brownian suspensions. This idea has been long established in the field of colloidal Brownian suspensions but is here extended to the case of concentrated non-Brownian suspensions and should be useful for the design of NBS in

many applications where rheology is crucial. Our current work focuses on expanding the range of monomers used in suspension copolymerization to afford polymer μ Ps with strikingly different compositions and thermomechanical properties. This may be particularly useful for the study of particle suspension dynamics. Suspension copolymerization led to μ Ps with alkyne groups distributed between the particle core and the surface and might therefore open the way to dually functionalized core-shell μ Ps. In hydroalcoholic medium, coupling through CuAAC occurs on the surface and performing a second functionalization step in organic medium should involve the alkyne groups located within particle core. Finally, better control of the μ Ps dimensions and dispersity using other emulsification processes is currently undergoing.

Acknowledgments

The authors gratefully acknowledge Veronica La Padula, Pierre Alcouffe and Valentin Cinquin and the CT μ microscopic center at University Lyon 1 for confocal fluorescence microscopy and SEM images. This work was supported by the Agence Nationale de la Recherche (ANR-18-CE06-0009).

Appendix A. Supplementary material

Supplementary data associated with this article can be found, in the online version, at ...

References

- [1] H. Kawaguchi, Functional polymer microspheres, *Prog. Polym. Sci.* 25 (2000) 1171–1210. [https://doi.org/10.1016/S0079-6700\(00\)00024-1](https://doi.org/10.1016/S0079-6700(00)00024-1).
- [2] M.T. Gokmen, F.E. Du Prez, Porous polymer particles - A comprehensive guide to synthesis, characterization, functionalization and applications, *Prog. Polym. Sci.* 37 (2012) 365–405. <https://doi.org/10.1016/j.progpolymsci.2011.07.006>.
- [3] J.J. Stickel, R.L. Powell, Fluid mechanics and rheology of dense suspensions, *Annu. Rev. Fluid Mech.* 37 (2005) 129–149. <https://doi.org/10.1146/annurev.fluid.36.050802.122132>.
- [4] I.E. Zarraga, D.A. Hill, D.T. Leighton, The characterization of the total stress of concentrated suspensions of noncolloidal spheres in Newtonian fluids, *J. Rheol. (N. Y. N. Y.)* 44 (2000) 185–220. <https://doi.org/10.1122/1.551083>.
- [5] M.M. Denn, J.F. Morris, Rheology of Non-Brownian Suspensions, *Annu. Rev. Chem. Biomol. Eng.* 5 (2014) 203–228. <https://doi.org/10.1146/annurev-chembioeng-060713-040221>.
- [6] R.I. Tanner, Review Article: Aspects of non-colloidal suspension rheology, *Phys. Fluids.* 30 (2018). <https://doi.org/10.1063/1.5047535>.
- [7] F. Gadala- Maria, A. Acrivos, Shear- Induced Structure in a Concentrated Suspension of Solid Spheres, *J. Rheol. (N. Y. N. Y.)* 24 (1980) 799–814. <https://doi.org/10.1122/1.549584>.
- [8] A. Singh, P.R. Nott, Experimental measurements of the normal stresses in sheared Stokesian suspensions, *J. Fluid Mech.* 490 (2003) 293–320. <https://doi.org/10.1017/S0022112003005366>.

- [9] S.-C. Dai, E. Bertevas, F. Qi, R.I. Tanner, Viscometric functions for noncolloidal sphere suspensions with Newtonian matrices, *J. Rheol. (N. Y. N. Y.)*. 57 (2013) 493–510. <https://doi.org/10.1122/1.4774325>.
- [10] É. Guazzelli, O. Pouliquen, Rheology of dense granular suspensions, *J. Fluid Mech.* 852 (2018) 61. <https://doi.org/10.1017/jfm.2018.548>.
- [11] F. Boyer, É. Guazzelli, O. Pouliquen, Unifying suspension and granular rheology, *Phys. Rev. Lett.* 107 (2011) 1–5. <https://doi.org/10.1103/PhysRevLett.107.188301>.
- [12] S. Gallier, E. Lemaire, F. Peters, L. Lobry, Rheology of sheared suspensions of rough frictional particles, *J. Fluid Mech.* 757 (2014) 514–549. <https://doi.org/10.1017/jfm.2014.507>.
- [13] F. Peters, G. Ghigliotti, S. Gallier, F. Blanc, E. Lemaire, L. Lobry, Rheology of non-Brownian suspensions of rough frictional particles under shear reversal: A numerical study, *J. Rheol. (N. Y. N. Y.)*. 60 (2016) 715–732. <https://doi.org/10.1122/1.4954250>.
- [14] W. Chèvremont, B. Chareyre, H. Bodiguel, Quantitative study of the rheology of frictional suspensions: Influence of friction coefficient in a large range of viscous numbers, *Phys. Rev. Fluids.* 4 (2019) 1–17. <https://doi.org/10.1103/PhysRevFluids.4.064302>.
- [15] G. Chatté, J. Comtet, A. Niguès, L. Bocquet, A. Siria, G. Ducouret, F. Lequeux, N. Lenoir, G. Ovarlez, A. Colin, Shear thinning in non-Brownian suspensions, *Soft Matter.* 14 (2018) 879–893. <https://doi.org/10.1039/c7sm01963g>.
- [16] L. Lobry, E. Lemaire, F. Blanc, S. Gallier, L. Lobry, E. Lemaire, F. Blanc, S. Gallier, F. Peters, L. Lobry, E. Lemaire, Shear thinning in non-Brownian suspensions explained by variable friction between particles, *J. Fluid Mech.* 860 (2019) 682–710. <https://doi.org/10.1017/jfm.2018.881>.
- [17] R. V. More, A.M. Ardekani, Effect of roughness on the rheology of concentrated non-Brownian suspensions: A numerical study, *J. Rheol. (N. Y. N. Y.)*. 64 (2020) 67–80. <https://doi.org/10.1122/1.5097794>.
- [18] V. Chaudhary, S. Sharma, Suspension polymerization technique: parameters affecting polymer properties and application in oxidation reactions, *J. Polym. Res.* 26 (2019). <https://doi.org/10.1007/s10965-019-1767-8>.
- [19] B. Brooks, Suspension polymerization processes, *Chem. Eng. Technol.* 33 (2010) 1737–1744. <https://doi.org/10.1002/ceat.201000210>.
- [20] P.J. Dowding, B. Vincent, Suspension polymerisation to form polymer beads, *Colloids Surfaces A Physicochem. Eng. Asp.* 161 (2000) 259–269. [https://doi.org/10.1016/S0927-7757\(99\)00375-1](https://doi.org/10.1016/S0927-7757(99)00375-1).
- [21] M. Alroaithi, F. Jahanzad, S. Sajjadi, Suppressing Coalescence and Improving Uniformity of Polymer Beads in Suspension Polymerization Using a Two-Stage Stirring Protocol, *Ind. Eng. Chem. Res.* 57 (2018) 11883–11892. <https://doi.org/10.1021/acs.iecr.8b01599>.
- [22] C.M. Cordoví, A. De Lucas, J.F. Rodriguez, J. Tejada, Influence of stirring speed on the suspension copolymerization of styrene with methyl methacrylate, *J. Macromol. Sci. - Pure Appl. Chem.* 34 (1997) 1339–1351. <https://doi.org/10.1080/10601329708011048>.
- [23] S. Mane, S. Ponrathnam, N. Chavan, Effect of Chemical Crosslinking on Properties of Polymer Microbeads: A Review, *Can. Chem. Trans.* 3 (2016) 473–485. <https://doi.org/10.13179/canchemtrans.2015.03.04.0245>.
- [24] S. Mane, Effect of Porogens (Type and Amount) on Polymer Porosity: A Review, *Can. Chem. Trans.* 4 (2016) 210–225. <https://doi.org/10.13179/canchemtrans.2016.04.02.0304>.
- [25] S. Mane, Functional Polymers: A Review, *Can. Chem. Trans.* 4 (2016) 316–327. <https://doi.org/10.13179/canchemtrans.2016.04.03.0307>.
- [26] P. Theato, H.A. Klok, *Functional Polymers by Post-Polymerization Modification*, First Edit, Wiley, 2013. <https://doi.org/10.1002/9783527655427>.
- [27] H.C. Kolb, M.G. Finn, K.B. Sharpless, Click Chemistry: Diverse Chemical Function from a Few Good Reactions, *Angew. Chemie - Int. Ed.* 40 (2001) 2004–2021. <https://doi.org/10.1002/1521->

- 3773(20010601)40:11<2004::AID-ANIE2004>3.0.CO;2-5.
- [28] W. Xi, T.F. Scott, C.J. Kloxin, C.N. Bowman, Click chemistry in materials science, *Adv. Funct. Mater.* 24 (2014) 2572–2590. <https://doi.org/10.1002/adfm.201302847>.
- [29] V. Castro, H. Rodríguez, F. Albericio, CuAAC: An Efficient Click Chemistry Reaction on Solid Phase, *ACS Comb. Sci.* 18 (2016) 1–14. <https://doi.org/10.1021/acscombsci.5b00087>.
- [30] M. Arslan, G. Acik, M.A. Tasdelen, The emerging applications of click chemistry reactions in the modification of industrial polymers, *Polym. Chem.* 10 (2019) 3806–3821. <https://doi.org/10.1039/c9py00510b>.
- [31] A. Tăbăcaru, B. Furdui, I.O. Ghinea, G. Cârâc, R.M. Dinică, Recent advances in click chemistry reactions mediated by transition metal based systems, *Inorganica Chim. Acta.* 455 (2017) 329–349. <https://doi.org/10.1016/j.ica.2016.07.029>.
- [32] N. Anwar, A. Rix, W. Lederle, A.J.C. Kuehne, RGD-decorated conjugated polymer particles as fluorescent biomedical probes prepared by Sonogashira dispersion polymerization, *Chem. Commun.* 51 (2015) 9358–9361. <https://doi.org/10.1039/c4cc10092a>.
- [33] A.S. Goldmann, A. Walther, L. Nebhani, R. Joso, D. Ernst, K. Loos, C. Barner-Kowollik, L. Barner, A.H.E. Müller, Surface modification of poly(divinylbenzene) microspheres via thiol-ene chemistry and alkyne-azide click reactions, *Macromolecules.* 42 (2009) 3707–3714. <https://doi.org/10.1021/ma900332d>.
- [34] L. Nebhani, S. Sinnwell, A.J. Inglis, M.H. Stenzel, C. Barner-Kowollik, L. Barner, Efficient surface modification of divinylbenzene microspheres via a combination of RAFT and hetero diels-alder chemistry, *Macromol. Rapid Commun.* 29 (2008) 1431–1437. <https://doi.org/10.1002/marc.200800244>.
- [35] K. Ouadahi, E. Allard, B. Oberleitner, C. Larpent, Synthesis of azide-functionalized nanoparticles by microemulsion polymerization and surface modification by click chemistry in aqueous medium, *J. Polym. Sci. Part A Polym. Chem.* 50 (2012) 314–328. <https://doi.org/10.1002/pola.25035>.
- [36] C.E. Evans, P.A. Lovell, Click chemistry as a route to surface functionalization of polymer particles dispersed in aqueous media, *Chem. Commun.* (2009) 2305–2307. <https://doi.org/10.1039/b821758k>.
- [37] D.R. Breed, R. Thibault, F. Xie, Q. Wang, C.J. Hawker, D.J. Pine, Functionalization of polymer microspheres using click chemistry, *Langmuir.* 25 (2009) 4370–4376. <https://doi.org/10.1021/la801880u>.
- [38] A. Bayraktar, B. Saraçoğlu, Ç. Gölgelioğlu, A. Tuncel, Click-chemistry for surface modification of monodisperse-macroporous particles, *J. Colloid Interface Sci.* 365 (2012) 63–71. <https://doi.org/10.1016/j.jcis.2011.08.071>.
- [39] A.S. Goldmann, L. Barner, M. Kaupp, A.P. Vogt, C. Barner-Kowollik, Orthogonal ligation to spherical polymeric microparticles: Modular approaches for surface tailoring, *Prog. Polym. Sci.* 37 (2012) 975–984. <https://doi.org/10.1016/j.progpolymsci.2011.11.008>.
- [40] O.Z. Durham, H.R. Norton, D.A. Shipp, Functional polymer particles via thiol-ene and thiol-yne suspension “click” polymerization, *RSC Adv.* 5 (2015) 66757–66766. <https://doi.org/10.1039/c5ra12553g>.
- [41] R.A. Prasath, M.T. Gokmen, P. Espeel, F.E. Du Prez, Thiol-ene and thiol-yne chemistry in microfluidics: A straightforward method towards macroporous and nonporous functional polymer beads, *Polym. Chem.* 1 (2010) 685–692. <https://doi.org/10.1039/c0py00041h>.
- [42] M.T. Gokmen, J. Brassinne, R.A. Prasath, F.E. Du Prez, Revealing the nature of thio-click reactions on the solid phase, *Chem. Commun.* 47 (2011) 4652–4654. <https://doi.org/10.1039/c0cc05340f>.
- [43] T. Kaufmann, M.T. Gokmen, S. Rinnen, H.F. Arlinghaus, F. Du Prez, B.J. Ravoo, Bifunctional Janus beads made by “sandwich” microcontact printing using click chemistry, *J. Mater. Chem.* 22 (2012) 6190–6199. <https://doi.org/10.1039/c2jm16807c>.
- [44] T. Kaufmann, C. Wendeln, M.T. Gokmen, S. Rinnen, M.M. Becker, H.F. Arlinghaus, F. Du Prez, B.J. Ravoo, Chemically orthogonal trifunctional Janus beads by photochemical “sandwich” microcontact

- printing, *Chem. Commun.* 49 (2013) 63–65. <https://doi.org/10.1039/c2cc36483b>.
- [45] H. Gao, K. Matyjaszewski, Synthesis of molecular brushes by “grafting onto” method: Combination of ATRP and click reactions, *J. Am. Chem. Soc.* 129 (2007) 6633–6639. <https://doi.org/10.1021/ja0711617>.
- [46] R.J. Phillips, R.C. Armstrong, R.A. Brown, A.L. Graham, J.R. Abbott, A constitutive equation for concentrated suspensions that accounts for shear-induced particle migration, *Phys. Fluids A*. 4 (1992) 30–40. <https://doi.org/10.1063/1.858498>.
- [47] A.W. Chow, S.W. Sinton, J.H. Iwamiya, T.S. Stephens, Shear-induced particle migration in Couette and parallel-plate viscometers: NMR imaging and stress measurements, *Phys. Fluids*. 6 (1994) 2561–2576. <https://doi.org/10.1063/1.868147>.
- [48] D. Merhi, E. Lemaire, G. Bossis, F. Moukalled, Particle migration in a concentrated suspension flowing between rotating parallel plates: Investigation of diffusion flux coefficients, *J. Rheol. (N. Y. N. Y.)*. 49 (2005) 1429–1448. <https://doi.org/10.1122/1.2079247>.
- [49] M. Keentok, S.C. Xue, Edge fracture in cone-plate and parallel plate flows, *Rheol. Acta*. 38 (1999) 321–348. <https://doi.org/10.1007/s003970050184>.
- [50] R.B. Bird, R.C. Armstrong, O. Hassager, *Dynamics of Polymeric Liquids*, Vol. 1: Fl, 1987. <http://www.amazon.com/Dynamics-Polymeric-Liquids-Mechanics-Polymer/dp/047180245X>.
- [51] F. Blanc, F. Peters, E. Lemaire, Local transient rheological behavior of concentrated suspensions, *J. Rheol. (N. Y. N. Y.)*. 55 (2011) 835–854. <https://doi.org/10.1122/1.3582848>.
- [52] M. Chanda, *Plastics Technology Handbook*, Fifth Edit, CRC Press, 2017. <https://doi.org/10.1201/9781315155876>.
- [53] T. Ishizone, G. Ueharai, A. Hirao, S. Nakhama, K. Tsuda, Anionic polymerization of monomers containing functional groups, 11, *Macromol. Chem. Phys.* (1997) 1827–1834. [https://doi.org/10.1022-1352/98/0909-1827\\$17.50+.50/0](https://doi.org/10.1022-1352/98/0909-1827$17.50+.50/0).
- [54] G. Boutevin, J.J. Robin, B. Boutevin, B. Ameduri, Synthesis and thermal properties of bismaleate and bisfumarate telechelic oligomers from hydroxytelechelic polybutadienes, *J. Appl. Polym. Sci.* 90 (2003) 72–79. <https://doi.org/10.1002/app.12556>.
- [55] F. Jahanzad, S. Sajjadi, B.W. Brooks, On the evolution of particle size average and size distribution in suspension polymerization processes, *Macromol. Symp.* 206 (2004) 255–262. <https://doi.org/10.1002/masy.200450220>.
- [56] F. Jahanzad, S. Sajjadi, B. Brooks, Suspension polymerisation in the presence of an inhibitor; Prolonged transition stage and suppressed emulsion particle formation, *Polymer (Guildf)*. 54 (2013) 16–23. <https://doi.org/10.1016/j.polymer.2012.10.050>.
- [57] O.H. Gonçalves, R.A.F. Machado, P.H.H. de Araújo, J.M. Asua, Secondary particle formation in seeded suspension polymerization, *Polymer (Guildf)*. 50 (2009) 375–381. <https://doi.org/10.1016/j.polymer.2008.11.006>.
- [58] Y. Almog, M. Levy, Dispersion Polymerization of Styrene: Effect of Surfactant., *J. Polym. Sci. A1*. 19 (1981) 115–126. <https://doi.org/10.1002/pol.1981.170190112>.
- [59] B.W. Brooks, Basic aspects and recent developments in suspension polymerisation, *Makromol. Chemie. Macromol. Symp.* 35–36 (1990) 121–140. <https://doi.org/10.1002/masy.19900350110>.
- [60] N. Kim, E.D. Sudol, V.L. Dimonie, M.S. El-Aasser, Poly(vinyl alcohol) stabilization of acrylic emulsion polymers using the miniemulsion approach, *Macromolecules*. 36 (2003) 5573–5579. <https://doi.org/10.1021/ma034037q>.
- [61] W.D. Sharpless, P. Wu, T.V. Hansen, J.G. Lindberg, Just click it: Undergraduate procedures for the copper(I)-catalyzed formation of 1,2,3-triazoles from azides and terminal acetylenes, *J. Chem. Educ.* 82 (2005) 1833–1836. <https://doi.org/10.1021/ed082p1833>.
- [62] R.V. Ostaci, D. Damiron, S. Al Akhrass, Y. Grohens, E. Drockenmuller, Poly(ethylene glycol) brushes grafted to silicon substrates by click chemistry: Influence of PEG chain length, concentration in the

- grafting solution and reaction time, *Polym. Chem.* 2 (2011) 348–354. <https://doi.org/10.1039/c0py00251h>.
- [63] J.F. Moulder, W.F. Stickle, P.E. Sobol, K.D. Bomben, *Handbook of X-ray Photoelectron Spectroscopy: A Reference Book of Standard Spectra for Identification and Interpretation of XPS Data*, 1992.
- [64] A. Saad, M. Abderrabba, M.M. Chehimi, X-ray induced degradation of surface bound azido groups during XPS analysis, *Surf. Interface Anal.* 49 (2017) 340–344. <https://doi.org/10.1002/sia.6113>.
- [65] R. Seto, R. Mari, J.F. Morris, M.M. Denn, Discontinuous shear thickening of frictional hard-sphere suspensions, *Phys. Rev. Lett.* 111 (2013) 1–5. <https://doi.org/10.1103/PhysRevLett.111.218301>.
- [66] C. Clavuda, A. Be-ruta, B. Metzgera, Y. Forterrea, Revealing the frictional transition in shear-thickening suspensions, *Proc. Natl. Acad. Sci. U. S. A.* 114 (2017) 5147–5152. <https://doi.org/10.1073/pnas.1703926114>.
- [67] J.Y. Moon, S. Dai, L. Chang, J.S. Lee, R.I. Tanner, The effect of sphere roughness on the rheology of concentrated suspensions, *J. Nonnewton. Fluid Mech.* 223 (2015) 233–239. <https://doi.org/10.1016/j.jnnfm.2015.07.007>.
- [68] R.I. Tanner, S. Dai, Particle roughness and rheology in noncolloidal suspensions, *J. Rheol. (N. Y. N. Y.)* 60 (2016) 809–818. <https://doi.org/10.1122/1.4954643>.
- [69] C. Hoyle, S. Dai, R. Tanner, A. Jabbarzadeh, Effect of particle roughness on the rheology of suspensions of hollow glass microsphere particles, *J. Nonnewton. Fluid Mech.* 276 (2020) 104235. <https://doi.org/10.1016/j.jnnfm.2020.104235>.
- [70] J.A. Richards, B.M. Guy, E. Blanco, M. Hermes, G. Poy, W.C.K. Poon, The role of friction in the yielding of adhesive non-brownian suspensions, *ArXiv.* 405 (2019). <https://doi.org/10.1122/1.5132395>.
- [71] A. Papadopoulou, J.J. Gillissen, H.J. Wilson, M.K. Tiwari, S. Balabani, Journal of Non-Newtonian Fluid Mechanics On the shear thinning of non-Brownian suspensions : Friction or adhesion ?, *J. Nonnewton. Fluid Mech.* 281 (2020) 104298. <https://doi.org/10.1016/j.jnnfm.2020.104298>.
- [72] R. Mari, R. Seto, J.F. Morris, M.M. Denn, Shear thickening, frictionless and frictional rheologies in non-Brownian suspensions, *J. Rheol. (N. Y. N. Y.)* 58 (2014) 1693–1724. <https://doi.org/10.1122/1.4890747>.
- [73] B.E. Guy, M. Hermes, W.E.E. Poon, Towards a Unified Description of the Rheology of Hard-Particle Suspensions, *Phys. Rev. Lett.* 115 (2015) 1–5. <https://doi.org/10.1103/PhysRevLett.115.088304>.
- [74] A. Singh, R. Mari, M.M. Denn, J.F. Morris, A constitutive model for simple shear of dense frictional suspensions, *ArXiv.* 457 (2017) 457–468. <https://doi.org/10.1122/1.4999237>.
- [75] P. Mocny, H.-A. Klok, Tribology of surface-grafted polymer brushes, *Mol. Syst. Des. Eng.* 1 (2016) 141–154. <https://doi.org/10.1039/C5ME00010F>.

Figure captions

Fig. 1. Monomers conversion as a function of polymerization time at 80 °C during the synthesis of μ Ps **MP1** by suspension polymerization (The solid line is intended only as a guide to the eye).

Fig. 2. (a-c) Optical microscopy images of alkyne-functionalized μ Ps **MP1**. (d) LD size distribution of μ Ps **MP1** (solid line) as well as μ Ps **MP1** replica (dotted line) and poly(ethylene glycol)-grafted μ Ps **MP3** (dashed line).

Fig. 3. (a-c) SEM images of alkyne-functionalized μ Ps **MP1** at different magnifications.

Fig. 4. Confocal fluorescence microscopy of equatorial cross-section (5 μ m thick) of (a) rhodamine-functionalized μ Ps **MP2** and (b) cresol red-functionalized μ Ps **MP6**.

Fig. 5. AFM (a-b) (20 \times 20 μ m²) 3D surface reconstruction, (c-d) (1 \times 1 μ m²) height and (e-f) (1 \times 1 μ m²) phase images of (a,c,e) alkyne-functionalized μ Ps **MP1** and (b,d,f) poly(ethylene glycol)-grafted μ Ps **MP3**.

Fig. 6. High resolution (a) I_{3d} and (b) N_{1s} of spectra of alkyne-functionalized μ Ps **MP1** (black line) and (1,2,3-triazolium)-grafted μ Ps **MP5** (red line). (c) Peak fitted high resolution of N_{1s} spectrum of μ Ps **MP5**. The N_{1s} curve (black line) was split into 3 signals with 1:1:1 area ratio for the 1,2,3-triazole groups (blue dashed lines) and 3 signals with 1:1:1 area ratio for the 1,2,3-triazolium groups (pink dashed lines). The red line corresponds to the sum of the different contributions.

Fig. 7. Shear viscosity vs shear stress for suspensions composed of either μ Ps alkyne-functionalized **MP1** (red dots), poly(ethylene glycol)-grafted **MP3** (blue dots) or (1,2,3-triazolium iodide)-functionalized **MP5** (black dots) for two particle volume fractions: (a) $\phi=0.40$ and (b) 0.44. The viscosity of the suspending liquid is 0.96 Pa s.

Schemes captions

Scheme 1. Synthesis of alkyne-functionalized cross-linked μ Ps **MP1**.

Scheme 2. Synthesis of rhodamine-functionalized μ Ps **MP2** and poly(ethylene glycol)-grafted μ Ps **MP3** by Click modification of alkyne-functionalized **MP1**.

Scheme 3. Synthesis of 1,2,3-triazolium-functionalized μ Ps **MP5** and **MP6** by *N*-alkylation and ion exchange reaction.

Supporting Information for

Cross-linked polymer microparticles with tunable surface properties by the combination of suspension free radical copolymerization and Click chemistry

Yoanh Moratille ^a, Muhammad Arshad ^c, Celine Cohen ^b, Abdelhamid Maali ^c, Elisabeth Lemaire ^b, Nathalie Sintès-Zydowicz ^{a,*}, Eric Drockenmuller ^{a,*}

^a Univ Lyon, Université Lyon 1, CNRS, Ingénierie des Matériaux Polymères, UMR 5223, F-69003, Lyon, France

^b Université Côte d'Azur, CNRS, InPhyNi-UMR 7010, 06108 Nice Cedex 2, France

^c Univ. Bordeaux, CNRS, LOMA, UMR 5798, F-33405, Talence, France

Determination of critical micelle concentration (C_{CMC})

Surface tensions (γ) of aqueous solutions were measured at 22 °C by the Wilhelmy plate method using a KRUSS tensiometer K100 and a platinum plate of 10 × 19.9 × 0.2 mm. Prior to each experiment, the instrument was calibrated by measuring the surface tension of distilled water ($\gamma = 72.7$ mN m⁻¹ at 22 °C). A 10.0 g L⁻¹ stock solution was prepared by dissolving PVA (100 mg, $M_w = 88\,000$ g mol⁻¹) in distilled water (10 mL) at 60 °C and was used to prepare 500, 200, 100, 75, 50, 10 and 1 mg L⁻¹ solutions. Before surface tension was measured, each solution was allowed to stand for 5 min and the platinum plate was always cleaned with distilled water followed by ethanol and heating with a burner. Each experiment was repeated three times and average values of the surface tension data were reported. Surface tension of solutions was plotted against surfactant concentration C_s (mol L⁻¹). The critical micelle concentration value C_{CMC} (mol L⁻¹) was determined by the intersection of the linear regression lines (Fig. S1). The plot of surface tension versus surfactant concentration was further used to estimate surface excess, Γ_s (mol m⁻²) using the Gibbs relation S1:

$$\Gamma_s = - \frac{1}{RT} \times \frac{d(\gamma)}{d(\ln C_s)} \quad (S1)$$

and from that, assuming that all the surfactant is at the interface, it is possible to determine m_s the minimum mass of surfactant required to stabilize a particular emulsion size using equation S2:

$$m_s = M_w \times (V_w \times C_{CMC} + A_{w/o} \times \Gamma_s) \quad (S2)$$

where R (J mol⁻¹ K⁻¹) is the universal gas constant, T (K) is the temperature and C_s is the bulk molar surfactant concentration and $d(\gamma)/d(\ln C_s)$ is the slope of the surface tension plot; M_w (g mol⁻¹) is the molar mass of PVA, V_w (L) is the volume of water in the emulsion and $A_{w/o}$ (m²) is the water/oil interfacial area within the emulsion calculated from the d_{50} diameter of the emulsion droplets.

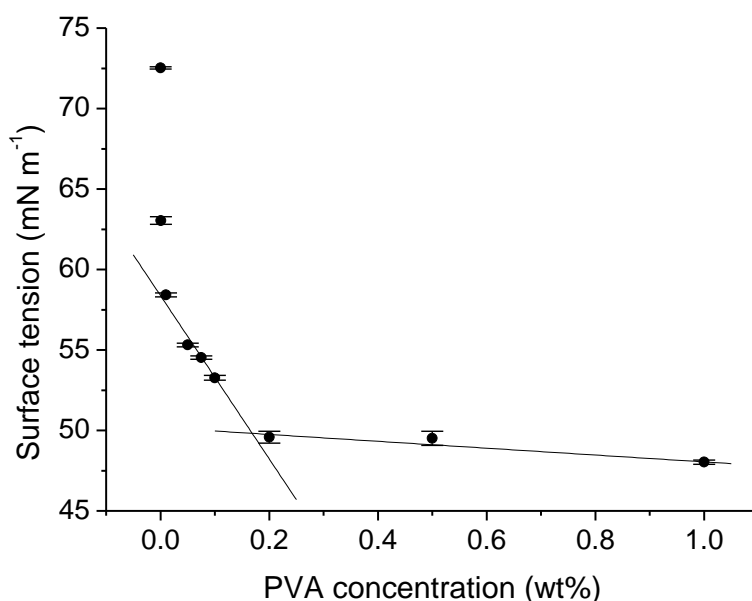


Fig. S1. Surface tension as a function of PVA concentration

Calculation of the number of surface alkyne functionalities

Considering the grafting density of azide-terminated PEG brushes on alkyne-functionalized polymer particles ranges from 0.017 to 0.5 chains nm⁻², the number of surface alkyne functionalities n_1 (mmol g⁻¹) at the surface of the μ Ps was determined using equation S3 [1–3]:

$$n_1 = \frac{D \times A \times N}{N_a} \quad (3)$$

$$N = \frac{m}{\rho \times V} \quad (4)$$

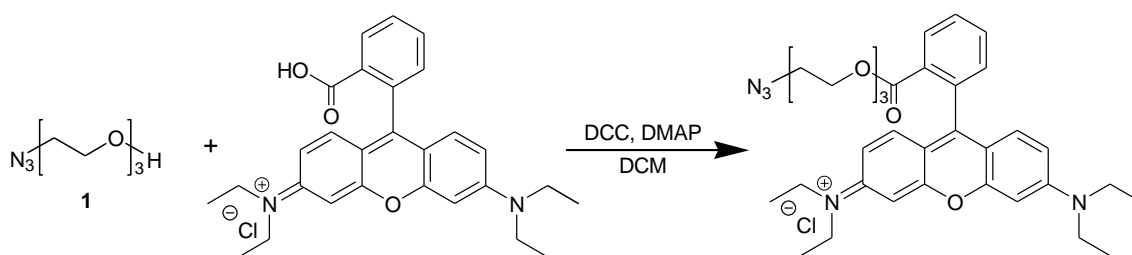
where D is the grafting density (chains nm⁻²), A is the surface area of a μ P with a diameter equal to the d_{50} diameter (80 μ m), N_a (mol⁻¹) is Avogadro's number; N is the number of μ Ps in the sample, m is the mass of the sample and ρ is the volumetric mass density of the μ Ps (1.045 g cm⁻³). Estimated number of surface alkyne functionalities n_1 lies between ca. 2.0×10^{-6} and 6.0×10^{-5} mmol g⁻¹.

Another estimation of the number of surface alkyne functionalities (n_2) can be made by considering the number of alkyne functionalities that can react with 2-[2-(2-azidoethoxy)ethoxy]ethanol **1** ($M_w = 37\,000$ g mol⁻¹) to form a ca. 10 nm thick dense layer of PEG brushes at the surface of the μ Ps using equation S5 :

$$n_2 = \frac{V \times \rho \times N}{M_w \times N_a} \quad (5)$$

here V is the volume of the layer formed by PEG (cm^3), ρ is the volumetric mass density of PEG and M_w is the molar mass of PEG. The number of surface alkyne functionalities n_2 is ca. $1.2 \times 10^{-5} \text{ mmol g}^{-1}$ equivalent to ca. $0.1 \text{ chain nm}^{-2}$.

From these methods, the estimated quantity of surface alkyne functionalities was fixed at n_2 and surface modification was carried out with an excess of azide reactant compared to n_2 (100 equiv.).



Scheme S1. Synthesis of azide-functionalized rhodamine B **2**.

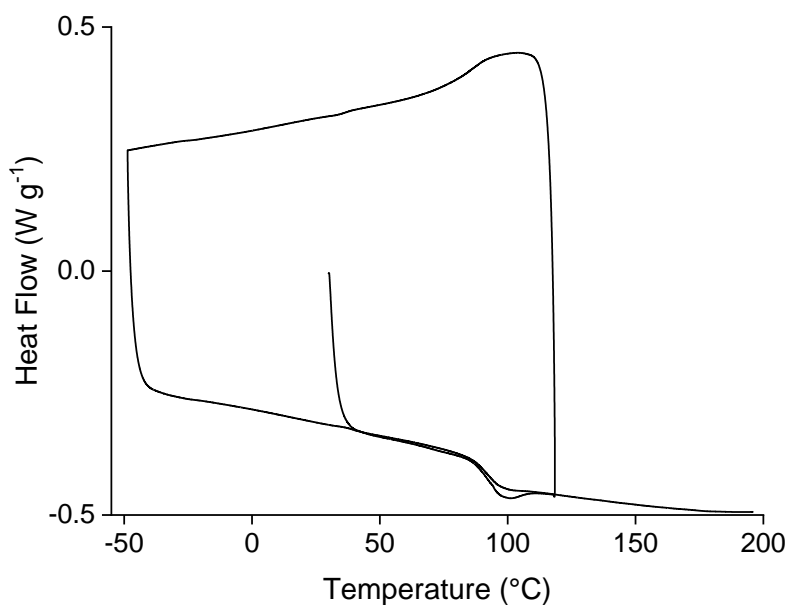


Fig. S2. DSC data of alkyne-functionalized μPs **MP1** obtained from the suspension copolymerization of styrene/HDDMA/PMA (85/5/10 mol%).

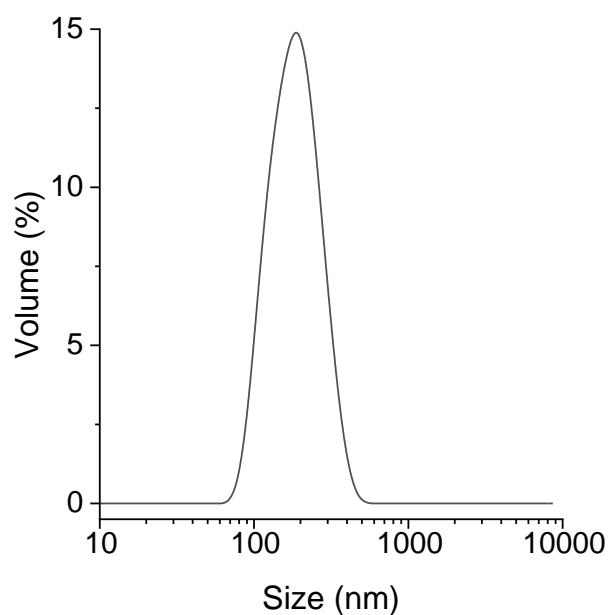


Fig. S3. DLS size distribution of emulsion particles in suspension polymerization of alkyne-functionalized μ Ps **MP1**.

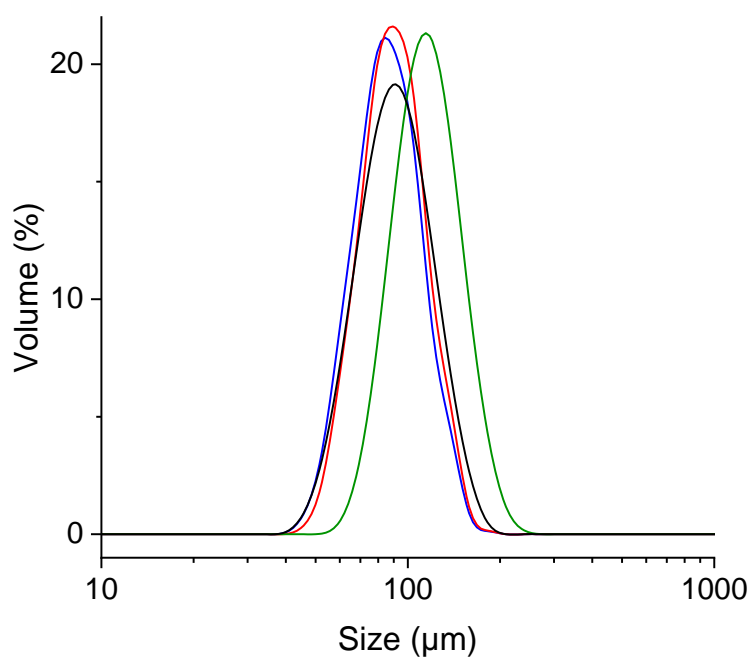


Fig. S4. LD size distribution of alkyne-functionalized μ Ps **MP1** after 72 h of immersion in water (blue line, $d_{50} = 80 \mu\text{m}$), EtOH (black line, $d_{50} = 83 \mu\text{m}$), CH₃CN (red line, $d_{50} = 84 \mu\text{m}$) and DCM (green line, $d_{50} = 107 \mu\text{m}$).

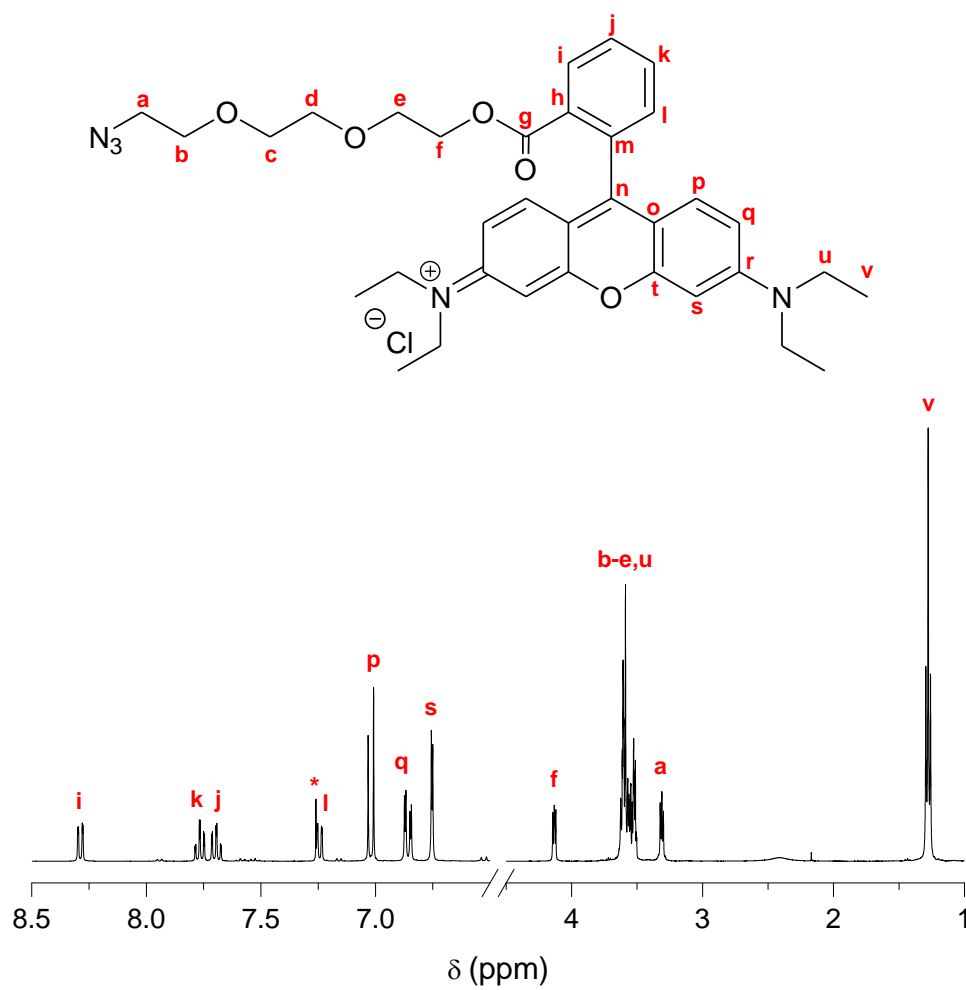


Fig. S5. ¹H NMR spectrum (25 °C, CDCl₃) of azide-functionalized rhodamine B 2 (*: peak assigned to CHCl₃).

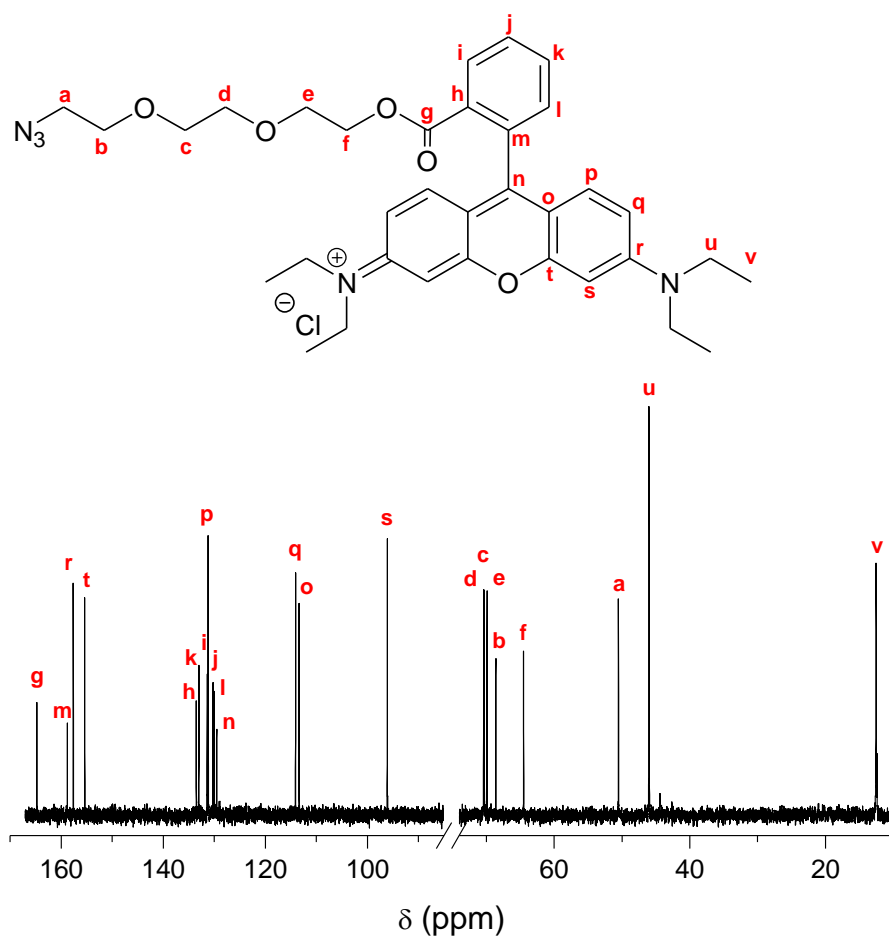


Fig. S6. ¹³C NMR spectrum (25 °C, CDCl₃) of azide-functionalized rhodamine B 2.

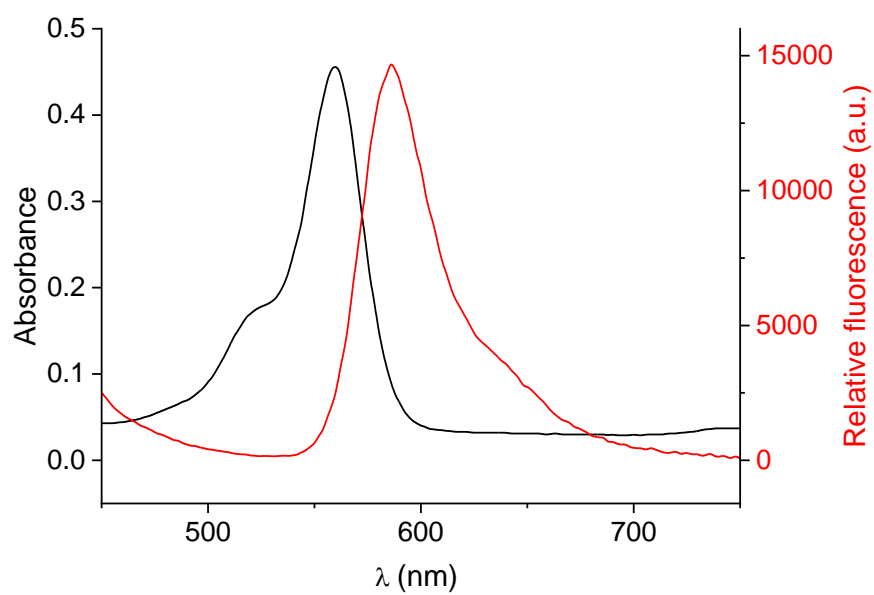


Fig. S7. UV-Vis absorption (black line, $\lambda_{\text{abs}} = 560$ nm) and emission (red line, $\lambda_{\text{abs}} = 586$ nm) spectra of azide 2 (10^{-3} mg mL⁻¹ in water at 25 °C).

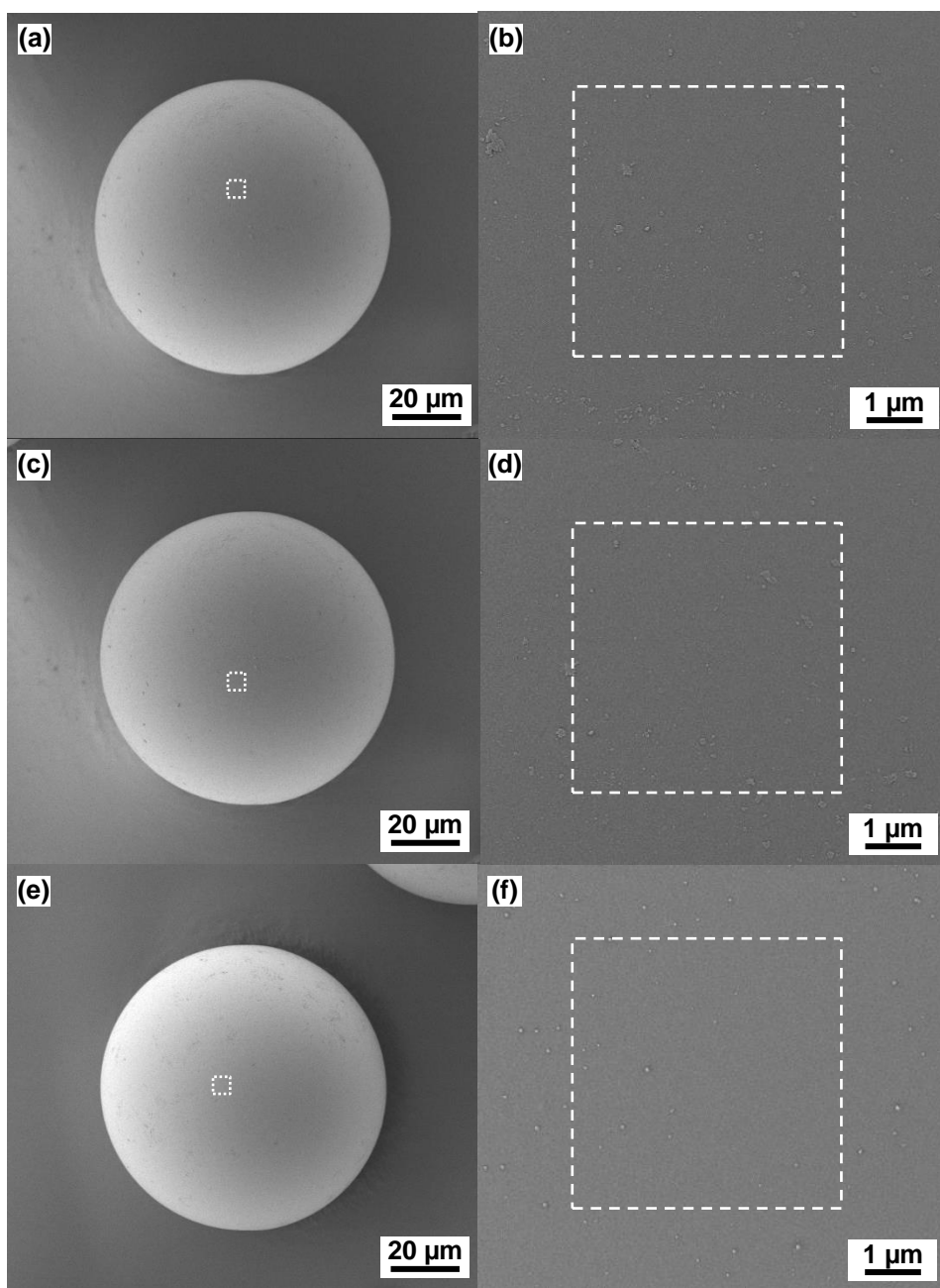


Fig. S8. SEM images of (a-b) poly(ethylene glycol)-grafted μP **MP3**, (c-d) tri(ethylene glycol)-grafted μPs **MP4** and (e-f) (1,2,3-triazolium iodide)-functionalized μP **MP5** at different magnifications.

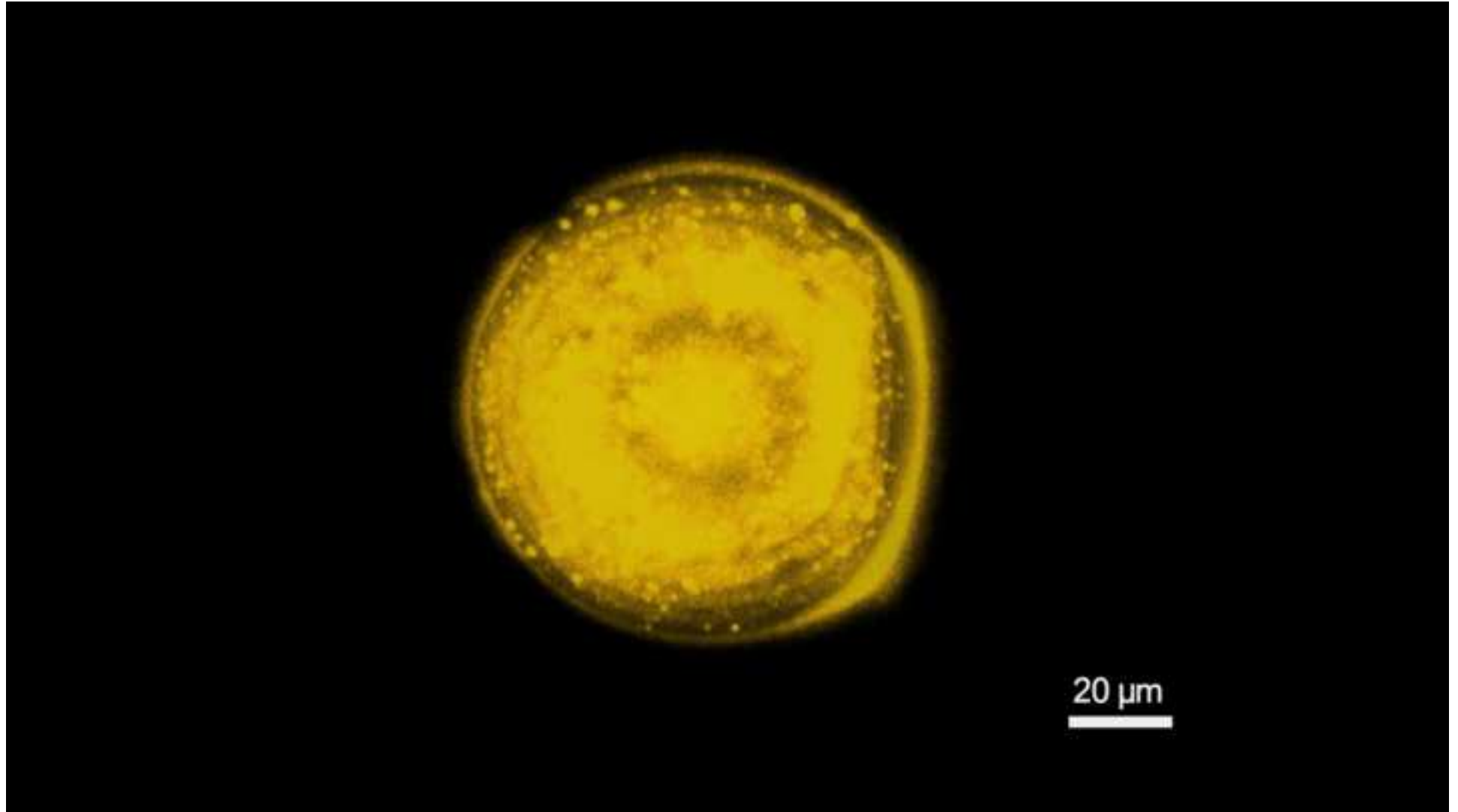
Table. S1. Water solubility of the monomers and initiator used for the preparation of alkyne-functionalized **MP1** μ Ps and estimation of their respective mass fraction contained in the aqueous phase.

	Water solubility (g L ⁻¹)	Mass fraction in the aqueous phase (wt%)	Reference
Styrene	0.27 (25 °C)	0.15	[4]
PMA	< 1.0 (20 °C)	3.9	*
HDDMA	0.023 (20 °C)	0.16	[6]
LPO	2.0×10^{-10}	2.4×10^{-8}	[7]

* No value in the literature, considered value is based on *N*-propyl methacrylate [5]

References

- [1] G.L. Li, R. Yu, T. Qi, H. Möhwald, D.G. Shchukin, Double-Shelled Polymer Nanocontainers Decorated with Poly(ethylene glycol) Brushes by Combined Distillation Precipitation Polymerization and Thiol-Yne Surface Chemistry, *Macromolecules*. 49 (2016) 1127–1134. <https://doi.org/10.1021/acs.macromol.5b02406>.
- [2] R.D. Roeder, P. Rungta, V. Tsyalkovskyy, Y. Bandera, S.H. Foulger, Colloidal templating: Seeded emulsion polymerization of a soluble shell with a controlled alkyne surface density, *Soft Matter*. 8 (2012) 5493–5500. <https://doi.org/10.1039/c2sm25070e>.
- [3] Y. Huang, T. Hou, X. Cao, Synthesis of silica-polymer hybrids by combination of RAFT polymerization and azide-alkyne cycloaddition ‘click’ reactions †, (2010) 1615–1623. <https://doi.org/10.1039/c0py00165a>.
- [4] J.E. Mark, *Polymer Data Handbook*, 1999.
- [5] L.H. Keith, D.B. Walters, *National Toxicology Program’s Chemical Solubility Compendium*, Third Edit, 2019. <https://doi.org/10.1016/B978-0-12-386454-3.01035-6>.
- [6] Evonick, Product information: Visiomer® 1,6-hddma, 3 (2020) 1–2. https://methyl-methacrylate-monomers.evonik.com/product/visiomer/downloads/vm011e_1_6hddma.pdf.
- [7] J.A. Alduncin, J. Forcada, A. José, Miniemulsion Polymerization Using Oil-Soluble Initiators, *Macromolecules*. 27 (1994) 2256–2261. <https://doi.org/10.1021/ma00086a041>.



Declaration of interests

The authors declare that they have no known competing financial interests or personal relationships that could have appeared to influence the work reported in this paper.

The authors declare the following financial interests/personal relationships which may be considered as potential competing interests: